Gondwana Research 64 (2018) 216–234

Contents lists available at ScienceDirect

Gondwana Research

journal homepage: www.elsevier.com/locate/gr

Predicted path for hotspot tracks off South America since Paleocene times: Tectonic implications of ridge-trench collision along the Andean margin

Juan Pablo Bello-González [a,*], Eduardo Contreras-Reyes [b], César Arriagada [a]

[a] Laboratorio de Paleomagnetismo, Departamento de Geología, Facultad de Ciencias Físicas y Matemáticas, Universidad de Chile, Santiago, Chile
[b] Departamento de Geofísica, Facultad de Ciencias Físicas y Matemáticas, Universidad de Chile, Santiago, Chile

ARTICLE INFO

Article history:
Received 12 January 2018
Received in revised form 20 July 2018
Accepted 23 July 2018
Available online 20 September 2018

Handling Editor: T. Gerya

Keywords:
Hotspot
Volcanism
Seamount
Plate reconstruction
Nazca
South America
Flat slab
Lithosphere

ABSTRACT

Hotspots are generated by partial melting due to hot plumes rising within the Earth's mantle, and when tectonic plates move relative to the plume source, hotspot tracks form. Off South America, the oceanic Nazca Plate hosts a large population of hotspot tracks. Examples include seamounts formed far from the Pacific-Nazca spreading center ("*off-ridge*" seamounts), such as the Juan Fernández Ridge (Juan Fernández hotspot), the Taltal Ridge (San Félix hotspot), and the Copiapó Ridge (Caldera hotspot). These hotspot tracks are characterized by a rough and discontinuous topography. Other examples include seamounts formed near the East Pacific Rise (EPR) ("*on-ridge*" seamounts), such as the Nazca Ridge (Salas y Gómez hotspot) and Easter Seamount Chain (Easter hotspot), and the Iquique Ridge (Foundation hotspot). These oceanic ridges developed a relatively smooth and broad morphology. Here, we present a plate reconstruction of these six oceanic hotspot tracks since the Paleocene, providing a kinematic model of ridge-continental margin collision. For the "*off-ridge*" seamount group, the plate kinematic reconstruction indicates that the collision point remained quasi-stationary from 40 to 30–25 Ma. Eventually, the southward migration of the collision point of this seamount group accelerated from 23 to 15 Ma (reaching a maxima speed of 300 km/Ma along the trench). From 15 Ma to present the collision point has remained quasi-stationary. The predicted location of the subducted portion of the Taltal, Copiapó and Juan Fernández Ridges coincides with the southward migrating (relative to South America) flat slab segment. For the "*on-ridge*" seamount group, the kinematic plate reconstruction indicates a continuous southward migration of the collision point from ~23 Ma, which is related to the fragmentation of the Farallon Plate. The southward migration accelerated until 15 Ma, reaching approximately 150 km/Ma. From 15 Ma to present, the southward migration has been decelerating except an increment of the migration velocity during the Chron 4 due to an increase of the convergence velocity. The migration velocity differences between the on-ridge and off-ridge hotspot tracks are mainly result from the hotspot track azimuth and the margin azimuth on the collision point. Convergence velocity varies along the trench, but it is a minor factor comparing different hotspot tracks migration velocity. Due to the EPR-plume interactions, our reconstruction suggests that the eastern Tuamotu Island Plateau formation occurred 48–27 Ma on the Easter Hotspot, which was located near to the EPR segment between the Marquesas and Austral Fracture Zones. Our model also predicts that the Iquique Ridge seamounts track is consistent with the position of the Foundation hotspot. The Foundation hotspot jumped to the Challenger (Resolution) Fracture Zone from the Farallon plate to the Pacific plate. This process triggered the cessation of the Iquique Ridge volcanic formation, and initiated volcanism at Foundation Chain in the Pacific Plate at ~25 Ma.

1. Introduction

Oceanic hotspot volcanism occurs due to the interaction of an overlying oceanic tectonic plate with a deep, hot mantle plume. Hotspots are relatively stationary and are characterized by large amounts of upwelling decompression melt that accumulates within the crust and upper mantle of the overlying oceanic plate, producing large volcanic eruptions at the seafloor (e.g., Morgan, 1972, 1978; Koppers and Watts, 2010). Oceanic hotspots are morphologically defined by a seamount track that progressively increases in age away from the active hotspot. They create broad regions of shallow seafloor, also known as "swells" (e.g., McNutt and Bonneville, 2000). "*On-ridge*" seamounts are characterized as broad, continuous and smooth ridges, and are often observed very close to the intersection of a hotspot plume and a spreading center. Seamounts formed in an "*off-ridge*" setting, far from a spreading center,

* Corresponding author.
E-mail address: jbello@ing.uchile.cl (J.P. Bello-González).

https://doi.org/10.1016/j.gr.2018.07.008
1342-937X/

are characterized by a rough and discontinuous topography (e.g., Orellana-Rovirosa and Richards, 2017). Geophysical and petrological constraints as well as physical models suggest that the smooth hotspot topography occurs when the overlying lithosphere is weak, thin, hot and young, allowing melt penetration and intrusive magmatism in the oceanic crust (Richards et al., 2013; Orellana-Rovirosa and Richards, 2017). In contrast, old, cold and rigid oceanic lithosphere may hinder intra-crustal melt penetration in an "intraplate" volcanic setting. In this case, a small fraction of the original magma succeeds in traversing the whole oceanic lithosphere through preexisting weak zones and fractures, and eventually reaches the surface by eruption (Orellana-Rovirosa and Richards, 2017).

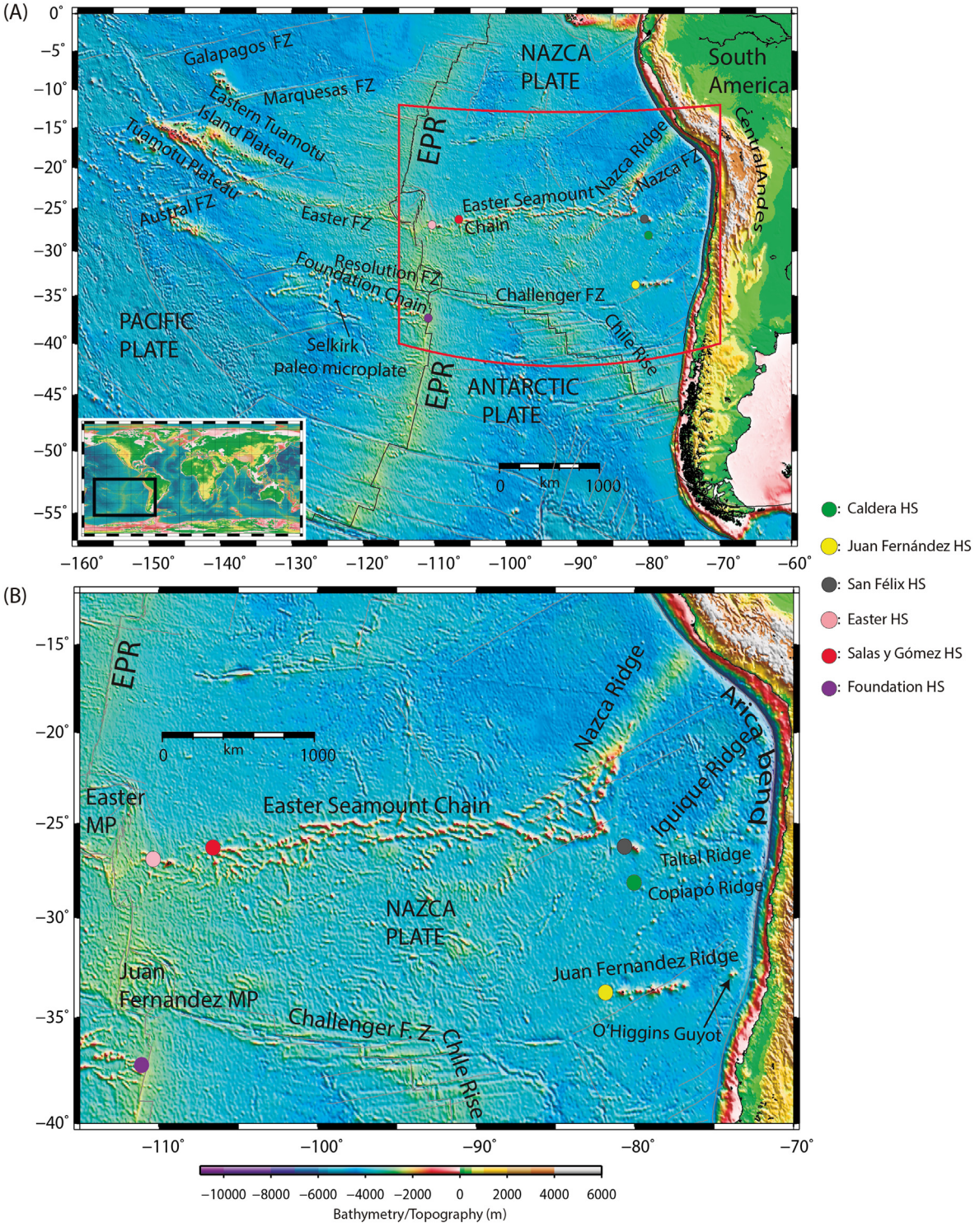

Fig. 1. (A) Present tectonic setting of Nazca plate hotspots. The colored dots represent the present location of the hotspots (HS). (B) The oceanic Nazca, Antarctic and Pacific plates are formed at the East Pacific Rise (EPR), and Nazca and Antarctic plates are formed at the Chile Rise, south of the Challenger Fracture Zone. Easter Microplate (MP) is adjacent to the EPR and Juan Fernandez MP is located at the Pacific-Nazca-Antarctic Triple Junction. The Easter Seamount Chain and Nazca Ridge were formed at the Sala y Gomez Hotspot and Easter Hotspot, in an on-ridge setting. The Iquique Ridge was likely formed at the Foundation Hotspot that also formed the Foundation Chain. The Juan Fernandez Ridge, Taltal Ridge, and Copiapó Ridge were formed at the Juan Fernández Hotspot, San Felix Hotspot, and Caldera Hotspot, respectively, in an off-ridge setting. The present location of the hotspots considered in this study is shown in Table 1 (Supplementary material).

Remarkably, the relatively small oceanic Nazca plate (off South America) hosts several hotspot tracks formed in "off-ridge" and "on-ridge" settings (Fig. 1). The Juan Fernández Ridge (e.g., Yáñez et al., 2001; Kopp et al., 2004) and the Copiapó Ridge (e.g., Álvarez et al., 2015) comprise the off-ridge hotspots, and the Carnegie and Malpelo Ridges (Sallarès et al., 2003), the Nazca Ridge (e.g., Hampel et al., 2004), and the Iquique Ridge (e.g., Rosenbaum et al., 2005) comprise the on-ridge hotspot tracks. For instance, the Nazca Ridge was formed by the Easter Island hotspot on or near the Pacific-Farallon/Nazca spreading center (also known as the East Pacific Rise) (Naar and Hey, 1986; Pilger, 1984; Steinberger, 2002; Ray et al., 2012), and is characterized by a seamount track ~1.5 km in average height surrounded by a topographic swell approximately 200–300 km wide (e.g., Hagen and Moberly, 1994; Hampel, 2002). Seismic constraints show that the Nazca Ridge is formed of anomalously thick oceanic crust (~17 km) and exhibits seismic velocities and densities similar to typical upper and lower oceanic crust (Hampel et al., 2004).

The subduction/collision of hotspot tracks play a major role in the long-term tectonic evolution of the outer forearc (Ballance et al., 1989; von Huene et al., 1997; Domínguez et al., 2000; Hampel et al., 2004, Spikings and Simpson, 2014) and on the short-term seismic cycle affecting earthquake rupture behavior at the subduction interface (e.g., Scholz and Small, 1997; Kodaira et al., 2000; Husen et al., 2002; Robinson et al., 2006; Anderson et al., 2007; Contreras-Reyes and Carrizo, 2011; Schellart and Rawlinson, 2013). Lithospheric-scale analog experiments and numerical 2D modeling have suggested that the formation of flat slab segments is the result of large buoyant ridges/plateaus forced to subduct by the trenchward advance of the overriding plate (Cloos, 1993; van Hunen et al., 2002; Gutscher et al., 2000; Espurt et al., 2008; Gerya et al., 2009; Spikings and Simpson, 2014; Hassani et al., 1997; Martinod et al., 2005; Vogt and Gerya, 2014; Huangfu et al., 2016; Hu et al., 2016). Flat subduction cools the subducting and overriding plates due to the absence of a hot asthenospheric wedge, which causes the cessation of calc-alkaline arc magmatism (McGeary et al., 1985; Kay and Abbruzzi, 1996). Rosenbaum and Mo (2011) argued that the recognition of these patterns could be useful for reconstructing oroclinal bending structures in both modern and ancient convergent plate boundaries.

Other works have founded alternative explanations of the flat slab developing. For instance, Rodríguez-González et al. (2012) proposed that the slab flattening is caused by the variation of the thickness of the overlying plate. On the other hand, Manea et al. (2012) have concluded that the Chilean flat slab area is the result of the combination of trenchward motion of thick cratonic lithosphere with trench retreat. This process is able to reproduce the temporal and spatial evolution of slab flattening and its associated upper plate deformation and volcanism. Similarly, Manea and Gurnis (2007) interpreted that a low viscosity mantle wedge or a low viscosity channel on top of the subducting slab have an important role in the Central Mexico flat slab segment.

Gutscher et al. (2000) suggested that higher interplate coupling in a flat slab geometry allows deformation transference for several hundred kilometers inland, resulting in large-scale block uplifts, as is present in the Sierras Pampeanas (Jordan et al., 1983; Smalley et al., 1993; Anderson et al., 2007). Thereby, the downdip limit for megathrust earthquakes could be extended for several km landward allowing events of major magnitudes (Gutscher et al., 1999). Alternatively, higher coupling and stronger rheology result in enhanced strain partitioning in cases of oblique convergence, as is present in the north Andes block, which is suggested by analog and numerical modeling (Pinet and Cobbold, 1992; Pubellier and Cobbold, 1996; Chemenda et al., 2000).

Skinner and Clayton (2013) argued the lack of correlation between flat slabs and the subduction of bathymetric features off South America. However, their reconstruction considered only on-ridge setting hotspot tracks. Another kinematic analysis (Schepers et al., 2017), has constrained the last 50 Ma NWN absolute motion of the western South American trench. These authors observed the present-day Pampean flat slab (Ramos and Folguera, 2009), whose length is spatially coincident with the amount of westward absolute Andean trench motion since the 12 Ma onset of flat slab formation. Thus, they concluded that the slab bend has been stationary in the mantle, and rollback was apparently impeded. Schepers et al. (2017) have proposed that this lasting 12 Ma mantle slab-stagnation is due to an overpressured sub-slab mantle that responds to any local decrease in subduction angle, initiated by one or more proposed flat slab triggers such as the subduction of hotspot tracks hosting anomalous oceanic crust (Pilger, 1981; Gutscher et al., 2000; van Hunen et al., 2000; Manea et al., 2012) to create and maintain a flat slab underlain by the overpressured sub-slab mantle.

Modeling the migration of subducting hotspot tracks along the western South American margin, and the study of the tectonostratigraphic record are useful to correlate the tectonic events that could be related to the subduction/collision of hotspot tracks, such as orogenic and uplift events (Pilger, 1984; Ballance et al., 1989; Domínguez et al., 2000; Hampel et al., 2004; Spikings and Simpson, 2014; Bello-González, 2015), volcanic activity, quiescence and magmatic geochemistry (Rosenbaum et al., 2005; Kay and Coira, 2009; McGeary et al., 1985; Gutscher et al., 2000; Yáñez et al., 2002; Araya, 2015), or metallogenic events (Cooke et al., 2005; Rosenbaum et al., 2005; Sun et al., 2010). In this paper, we present a kinematic reconstruction of the ridge-continent collision off the coast of South America, considering Juan Fernández, Copiapó, Taltal, Nazca, and Iquique ridges, as well as of the Eastern seamount chain since the Paleocene. The results are further discussed in terms of their geodynamic implications.

2. Plate tectonic setting

The Nazca plate presents the following characteristics: (1) it is placed at the eastern boundary of the fastest-spreading ocean ridge on Earth, the East Pacific Rise (EPR) (Fig. 1A), (2) the plate is bordered by two microplates, the Easter microplate and the Juan Fernandez microplate, and includes several relict microplates (e. g. Mendoza and Bauer) and three major seamount chains, the Easter Seamount Chain, the Nazca Ridge, and the Carnegie Ridge (e.g. Mayes et al., 1990; Naar and Hey, 1991; Liu, 1996) (Fig. 1), (3) it also contains several active hotspots. One of these hotspots is the Easter hotspot that corresponds to one of the few Pacific hotspots inferred by Courtillot et al. (2003) to have a deep, lower mantle origin, deeming the Easter hotspot a 'primary' hotspot.

The break-up of the Farallon Plate at Chron 6B (~22.7 Ma) (Barckhausen et al., 2001) resulted in the development of the Cocos-Nazca spreading system (Hey, 1977; Mayes et al., 1990) and consequently, the formation of the Nazca and Cocos plates (Hey, 1977; Barckhausen et al., 2001). The separation of the Farallon plate could be caused by a combination of tectonic factors. For instance, Lonsdale (2005) has attributed the Cocos-Nazca break-up to an increased northward pull after the previous fragmentation of the Farallon and Vancouver plates (Atwater, 1989) in the North Pacific, and an increase in slab pull at the Middle America subduction zone (Lonsdale, 2005). The Galapagos hotspot could have also contributed to the Farallon break-up by weakening the oceanic lithosphere due to a thermal anomaly caused by the Galapagos Plume (Hey, 1977; Lonsdale, 2005; Barckhausen et al., 2008). The Farallon plate fragmentation is a major plate reorganization event that must be considered to understand the tectonic evolution of the South Pacific. Plate reorganization generates changes in the plate motions. Indeed, these processes define the hotspot tracks, that are the most important factor to determinate the shape of the associated seamount chain. In the following, we describe the seamount chains observed in the Nazca Plate.

2.1. Easter Seamount Chain and Nazca Ridge

The total length of the Easter Seamount Chain and Nazca Ridge together is about 4100 km long (Fig. 1). The Easter Seamount Chain is

~2900 km long and ~150 km wide, and it trends roughly west-east, from near the East Rift spreading axis of the Easter Microplate to the southern end of the Nazca Ridge. The Nazca Ridge is ~1200 km long and 300 km wide, and it extends in a N42°E direction (Hampel, 2002) (Fig. 1), from the eastern end of the Easter Seamount Chain to the Peru-Chile Trench (e.g. Woods and Okal, 1994). The age of the 'elbow' in the Easter Seamount Chain-Nazca Ridge system, where the Nazca Ridge meets the Easter Seamount Chain, is 23 ± 1 Ma (e.g., Ray et al., 2012) (Fig. 2). This age corresponds to a change in absolute Pacific plate motion estimated at about 23 Ma by Wessel and Kroenke (2000) and may reflect the breakup of the Farallon plate into the Nazca and Cocos plates (e.g., Barckhausen et al., 2008; Ray et al., 2012).

Some authors propose that the Nazca Ridge and Tuamotu Plateau (Fig. 1A) were both formed by the Easter Island hotspot at the East Pacific Rise (Morgan, 1972; Pilger, 1984; Hampel, 2002), due to the congruent features of the two tectonic settings (Pilger, 1981; Rosenbaum et al., 2005). The subduction of the Nazca Ridge spatially correlates with a gap in arc volcanism and a relatively flat subduction angle of the down-going Nazca plate in Peru (e.g., McGeary et al., 1985; Gutscher et al., 2000).

Despite its importance as a major hotspot trail, most of the Easter Seamount Chain-Nazca Ridge system has neither been studied geochemically nor dated. Only a few volcanoes east of the Salas and Gómez Island have been sampled (Ray et al., 2012). Thus, many questions regarding the formation and evolution of the Easter Seamount Chain-Nazca Ridge system remain unanswered. In particular, questions concerning the present location of the hotspot center, the age of the system, the geochemical evolution of the hotspot source and melting conditions (i.e. depths and amounts of partial melting) that prevailed during the formation of the Nazca Ridge and the Easter Seamount Chain require a thorough investigation. Geochronological studies (Ray et al., 2012) show an age progression from the EPR to the trench, they predict that the Easter Seamount Chain and Nazca Ridge are part of the same, 30 Ma hotspot trail and is consistent with a hotspot center near Salas y Gomez Island, although the present location of the hotspot center is unclear. Samples extracted from Salas and Gómez Island have been dated from 1.3 to 1.9 Ma. On other hand, near the Easter Island that is located 400 km westward of the Salas and Gómez Island, samples have been dated from 0.13 to 2.4 Ma (Ray et al., 2012 and references therein). Thus, they could be two different hotspots tracks.

2.2. Iquique Ridge

The Iquique Ridge is composed of several seamounts (<1.5 km high) surrounded by a broad region of shallow seafloor, which is also known as swell. This swell is up to 250 km wide in some areas and >500 m in elevation (Contreras-Reyes and Carrizo, 2011, Fig. 1B). The Iquique Ridge is observed from the north of the Taltal Ridge to the intersection of the trench in the Arica bend, which is the location where the ridge is actually subducting (Figs. 1B and 2). The areal extent of the swell is not clear due to the presence of prominent outer rise topography (e.g., Contreras-Reyes and Carrizo, 2011). In addition, the swell topography of the Iquique Ridge is heterogeneous relative to the Nazca Ridge swell topography. The Iquique Ridge trends parallel to the Nazca Ridge, and it extends >1000 km across the oceanic Nazca plate (Fig. 1). The global elevation model (Amante and Eakins, 2009) shows a rough and discontinuous bathymetric seamount track from the north of the Challenger Fracture Zone to the Taltal Ridge (Figs. 2 and 3), this ridge trends the same direction as the Iquique Ridge and could be a south-west extension of the Iquique Ridge with a similar origin.

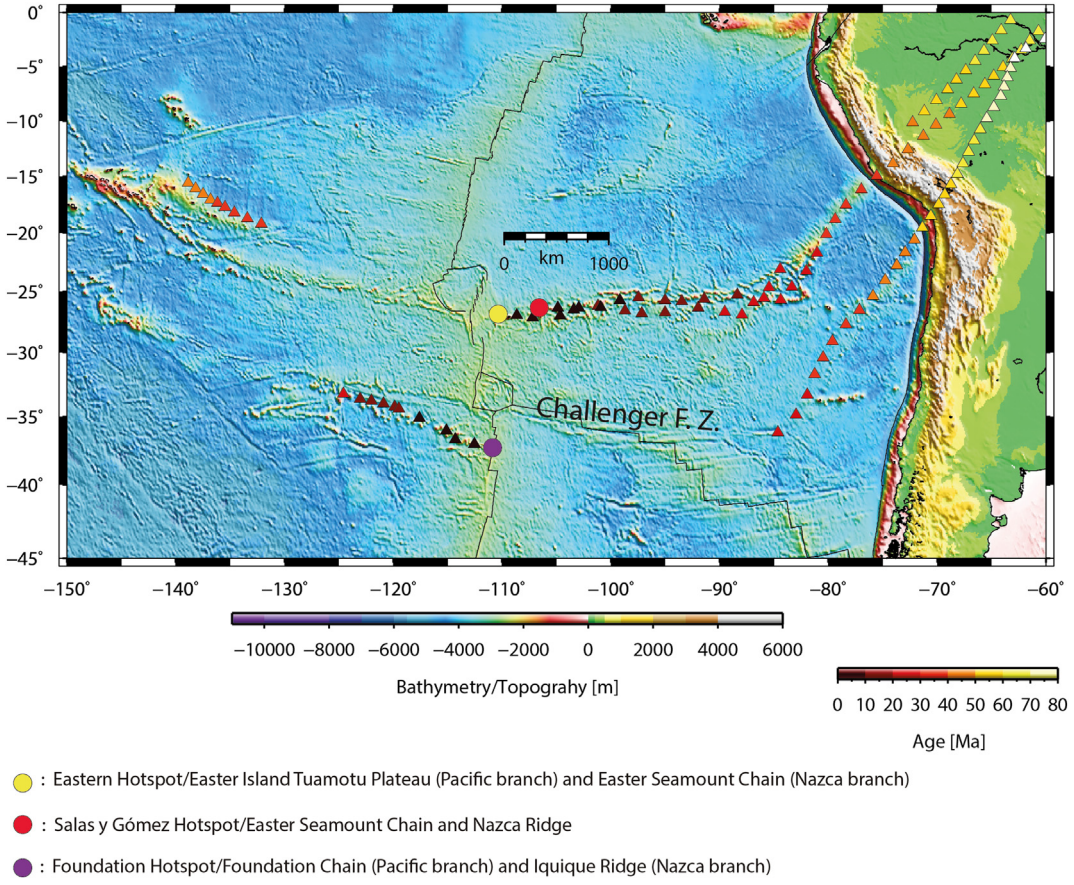

Fig. 2. Predicted path for the On-Ridge, Easter, Salas y Gómez, and Foundation hotspot tracks at present, based on the Farallon/Nazca Hotspot motions and Nazca Plate motions from rotations poles shown in Tables 2 and 3 (Supplementary Material, Model 1).

2.3. Copiapó Ridge

Contreras-Reyes and Carrizo (2011) proposed the existence of the Copiapó Ridge (Figs. 1 and 3), however there is no geochronological data of this seamount track so far. The trail of this seamount chain is clearly visible in bathymetry maps at 28.06°S, whereas the position of the present hotspot is at ~(28.06°S-80.18°W). In addition, there is geophysical and geological evidence that the Copiapó Ridge is currently subducting beneath the South American plate (Álvarez et al., 2015).

2.4. Taltal Ridge

The San Felix and San Ambrosio islands lie about 200 km SE of the ~23 Ma 'elbow' in the Easter Seamount Chain-Nazca Ridge system. Geochronological data obtained from San Félix Island shows an age of 0.421 ± 0.018 Ma (Haase et al., 2000). This implies that the magmatic event which generated this island has no relation with the mantle plumes that generated the Easter Seamount Chain-Nazca Ridge system (Figs. 1 and 3). It is more likely that San Félix island was generated more recently by another hotspot. This hypothesis is supported by the observation of the E-W seamount track to the east of San Félix island (Fig. 1), which also correlates with the last ~10 Ma Nazca Plate absolute motion (Fig. 3). This oceanic ridge, also known as the "Taltal Ridge", intersects with the trench at 25°S offshore near Taltal town (Contreras-Reyes and Carrizo, 2011).

The San Felix (SF) and San Ambrosio Islands belong to a single volcanic edifice. González-Ferrán (1987) dated a dike and a lava flow (2,86 ± 0,14 and 2,93 ± 0,15 Ma respectively) in San Ambrosio Island. The San Félix and San Ambrosio islands correspond to the expected stages of volcanism within their volcanic complex (Cooper and Lara, 2015). This is evident by the proximity between the San Félix and San Ambrosio islands (~20 km), the fact that they belong to the same volcanic shield, and the increase in alkalinity on the younger of the two islands (San Félix). Additionally, the maximum hiatus in age is a mere ~2.7 Ma, which is derived from the volcanic activity of San Ambrosio (~2.9 Ma) and San Félix (~0.2 Ma). There are no seamounts dated in the Taltal Ridge.

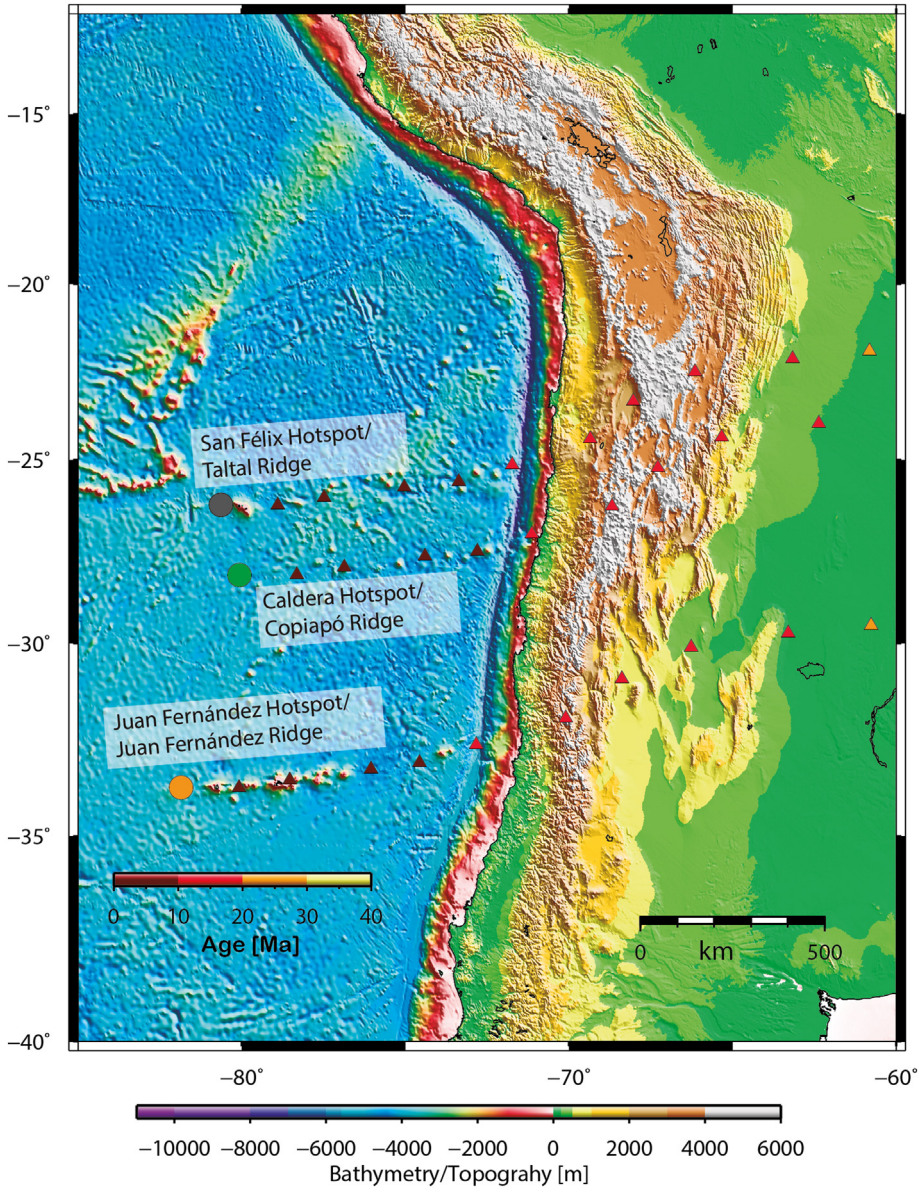

Fig. 3. Predicted path for the Off-Ridge, Juan Fernández, Caldera, and San Félix hotspot tracks at present, based on the Farallon/Nazca Hotspot motions and Nazca plate motions from rotations poles shown in Tables 2 and 3 (Supplementary Material, Model 1).

2.5. Juan Fernández Ridge

Geochronological data from lava samples obtained in the Archipelago Juan Fernández determine the age of Robinson Crusoe Island to be 1 to 4 Ma, and the Alejandro Selkirk Island located about 180 km eastward to be about 1 Ma (Reyes and Lara, 2012) (Fig. 3). These authors explain that the deviation in age obtained from the Robinson Crusoe Island is due to post-erosional magmatic episodes (Clague and Dalrymple, 1987) after the mantle plume activity that generated the basement of the island. The O'Higgins Guyot seamount is located ~100 km westwards of the trench axis, and its age is estimated at 8.5 ± 0.4 Ma by Yáñez et al. (2001) (Figs. 1 and 3). The hotspot origin for this oceanic ridge is determined by the eastward progression of age of the seamounts, which is constrained by magnetic data from the seafloor and ridge (Yáñez et al., 2001).

3. Methodology

Our plate reconstruction is based on the absolute plate motions in a reference frame defined by the global moving hotspot reference frame (GMHRF, Doubrovine et al., 2012). Because of the overall good fit of the GMHRF to the hot spot tracks in both the Indo-Atlantic and Pacific oceanic domains last 120 Ma and the statistically rigorous approach used to define the absolute rotations. The GMHRF corresponds to a "mean mantle" reference frame in which the convective motions within the mantle have been averaged to no net rotation (Steinberger and O'Connell, 1998; Steinberger, 2000). The analysis of the effects of bathymetric anomalies subduction in the Andean margin requires constraining Farallon/Nazca Plate and South America relative motion. We use the African absolute plate rotations and link them to a rotation hierarchy, that helped us to define two plate circuits from Africa to calculate de relative motion between subducting and overriding plates in the western South American trench. Our reconstruction considers the relative motion from: (1) South America-Africa plate circuits by Müller et al. (1999) and Heine et al. (2013) Atlantic rift reconstruction, and (2) Africa-East Antarctic-West Antarctic-(Pacific before 15.09 Ma)-Farallon/Nazca plate circuit, whose relative motion was taken from Royer and Chang (1991), Cande et al. (2010), Bernard et al. (2005), Nankivell (1997), Marks and Tikku (2001) and Müller et al. (2008) for the Antarctic-African spreading history. We also consider the West Antarctic-East Antarctic relative motion studied by Cande and Stock (2004), Granot et al. (2013) and Matthews et al. (2015). We adopt the Pacific-West Antarctic relative motion from Croon et al. (2008) and Wright et al. (2015, 2016). All these relative motion reconstructions were considered in order to be consistent with the Müller et al. (2016) global reconstruction. The Pacific Plate can be linked to the African plate circuit only for times later than chron 34y (83 Ma), based on the establishment of seafloor spreading between the Pacific and West Antarctic Plates (Müller et al., 2016). For the Pacific Plate motions during the chron 34y (83–120 Ma), we used the absolute rotations calculated by Doubrovine et al. (2012).

Two alternative models of the Farallon-Nazca hotspots location and EPR spreading history starting from 120 Ma were constructed for three main reasons: (1) Due to the lack of information available to model the plate boundaries of the Pacific Basin to previous ages in the generation of the Plateau Ontong Java Nui (Taylor, 2006), (2) the scarcity of information to model plate boundaries to the east of the EPR during the Super Chron 34 due the subduction of these plates below the South American plate, and (3) GMHRF implemented the Easter, San Felix and Juan Fernández hotspots absolute motions, which is useful to compare the hotspot track generated by these hotspots absolute motions, and our Farallon-Nazca fixed hotspots motion model.

Model 1 considers all hotspot shown in Fig. 1. The EPR spreading history was reconstructed in this work (0–47.9 Ma), the extrapolation of the current asymmetry shown by the EPR expansion modeled by Rowan and Rowley (2014) (50.78–83 Ma), and the rotational parameters of Farallon Plate calculated by Müller et al. (2016) (83–120 Ma). This Farallon/Nazca to Pacific relative plate motion is based on a compilation of magnetic anomaly identifications (Seton et al., 2014) fitted to the Gee and Kent (2007) time scale, and an interpretation of global and local fracture zones (FZ) (Tebbens and Cande, 1997; Matthews et al., 2011). Our 47.9 Ma to present EPR reconstruction was generated from oceanic crust polygons defined by isochrons and fracture zones, we adjusted our reconstruction considering the oceanic picks isochrons and oceanic bathymetry exhaustively.

In building our Farallon-Nazca hotspots motion model, we fitted the dated sample positions with the present bathymetric features and their reconstructed geometry by the rotation parameters for the kinematic model. We identified islands and seamounts with available geochronological data, and used the coordinates and ages of samples dated in the Nazca Ridge (Ray et al., 2012), the Taltal Ridge (Cooper and Lara, 2015) and the Juan Fernández Ridge (Astudillo, 2014) in order to reconstruct a Farallon/Nazca Plate Hotspot reference frame to generate the Model 1 hotspot tracks. The bathymetric data was extracted from the global elevation model of Amante and Eakins (2009). The rotational parameters of the Farallon-Nazca hotspots were fixed to the absolute plate motion of the Pacific hotspots before 40.1 Ma, which was previously modeled by Wessel and Kroenke (2008). We linked the Farallon/Nazca hotspots motion model with the Africa-East Antarctic-West Antarctic-Pacific-Nazca (Farallon) plate circuit (0–83 Ma) and with the Pacific Plate absolute hotspot motion of Doubrovine et al. (2012) for times older than 83 Ma. We emphasize that hotspot tracks generated during 120–83 Ma from this model should be considered carefully due to the absence of geomagnetic inversions (Superchron 34 of normal polarity) that generate magnetic isochrones to reconstruct the ocean basins accurately.

In order to set tectonically the Pacific Basin at the starting time of our model, we referred to the "120 Ma event" when a "superplume" that originated 125 Ma near the core/mantle boundary, and rose by convection through the entire mantle and erupted beneath the mid-Cretaceous Pacific basin (Larson, 1991). We modeled the location of the Farallon-Nazca hotspots starting from 120 Ma due to the lack of information available to model the plate boundaries of the Pacific Basin to previous ages in the generation of the Plateau Ontong Java Nui (Taylor, 2006). The scarcity of information to model plate boundaries to the east of the EPR during the Super Chron 34 is due to the subduction of these plates below the South American plate. This model assumes that the Pacific-Farallon-Phoenix plates triple junction jumped from the Nova-Canton trough to nearby the northeast corner of the Manihiki Plateau at 121–119 Ma, a process which resulted in the formation of Galapagos FZ (Larson and Pockalny, 1997; Larson et al., 2002; Viso et al., 2005), as well as rifting and fragmentation in the Manihiki Plateau (Larson et al., 2002; Viso et al., 2005; Taylor, 2006). One of these fragments rifted off to the east to the Farallon plate, and other rifted off to the south to the Phoenix plate. Some reconstructions (Kerr and Tarney, 2005; Bello-González, 2015; Hochmuth and Gohl, 2017) predict a possible subduction of these plateau fragments and a buildup of accretional margins off the coast of Ecuador. These predictions are supported by dating and geochemical studies in the Piñón Formation in Ecuador and the Antarctic Peninsula (Hochmuth and Gohl, 2017). The intersection of the Pacific–Ellice Basin rift boundary and Nova-Canton Trough north of Manihiki suggests that left-lateral motion along the rift boundary may have triggered the Nova-Canton Trough formation when Pacific–Farallon spreading initiated after the Pacific-Farallon-Phoenix triple junction jump (120 Ma, Chandler et al., 2012). Due to Ellice Basin spreading, Plateau Manihiki moved eastward around one thousand kilometers with respect to Ontong Java plateau between 119 and 83 Ma (Larson et al., 2002; Taylor, 2006; Chandler et al., 2012; Bello-González, 2015). The Model 1 does not consider a mid-oceanic ridge with nearly E-W orientation separating the Farallon from the Chasca Plate during Chron C34 (120–86 Ma) (Seton et al., 2012). In contrast, the model assumes asymmetric spreading, and is well constrained near the ridge axes in close

proximity to hotspots (Small, 1995; Müller et al., 1998), which is pertinent in this case.

Model 2 predicts only the Easter, San Félix and Juan Fernandez Hotspot tracks. This model considers the relative motion of the Nazca Plate calculated by Tebbens and Cande (1997) and Croon et al. (2008), and the Farallon-Pacific spreading history published by Müller et al. (2008) and Wright et al. (2015, 2016). Before the 86 Ma, we consider the Pacific Basin plate configuration of Seton et al. (2012). The hotspots studied in this work were mostly located in the Chasca Plate during 86–120 Ma proposed by Seton et al. (2012). Thus, the rotation parameters used to generate the hotspot tracks of Model 2 correspond to this hypothetic plate. The hotspot motions of Model 2 were modeled by Doubrovine et al. (2012) based on advecting plume conduits in the mantle flow field corresponding to the final iteration of the GMHRF. The plume parameters used for these calculations were modeled by Steinberger (2000) and Steinberger and Antretter (2006). We computed the stage rotation per each coordinate provide by Doubrovine et al. (2012) (Table S6 from their Auxiliary Dataset D1), of the Easter, San Félix and Juan Fernandez Hotspots. These rotations were determined by formulas detailed in Cox and Hart (1986, Chapter 7).

The both models' paths of motion have been calculated with the software GPlates (Boyden et al., 2011), with a starting age of 120 Ma and a time interval of 1 Ma. These files are available in our e-Component.

The western South American plate margin kinematics were reconstructed considering the Bolivian and Maipo oroclines stages at 40 Ma and 15 Ma, constrained by paleomagnetic data (Arriagada et al., 2008, 2013). We interpolated these orocline reconstructions and the present-day margin in 1 Ma intervals.

Intersection point of hotspot tracks with South American margin were analyzed since 60 Ma to present with a time interval of 1 Ma for both hotspot track reconstructions considering South America fixed (Model 1, Figs. 9A and 11; Model 2, Fig. 11 and Supplementary material Fig. S3). The aim of anchorage of South America is simplify analysis of our study comparing with local tectonic studies along the Andean margin. This calculation considered the interception point as the point defined by the interception between two great circles, one defined by the reconstructed margin segment, and the other circle defined by the hotspot track segment (Fig. 4).

We calculated the velocity at which the bathymetric high moves along an active margin at the interception point with the trench for each seamount track analyzed since 60 Ma to present, with a time interval of 1 Ma for the Model 1 (Fig. 9B). This calculation is based on the method described by Hampel (2002) (Fig. 5). We considered the azimuths of the seamount track and margin segments used to calculate the intersection points, and the azimuth and velocity of the convergence vector between the Farallon-Nazca plate, keeping the South America Craton fixed (Model 1, Fig. 10; Model 2, Supplementary material

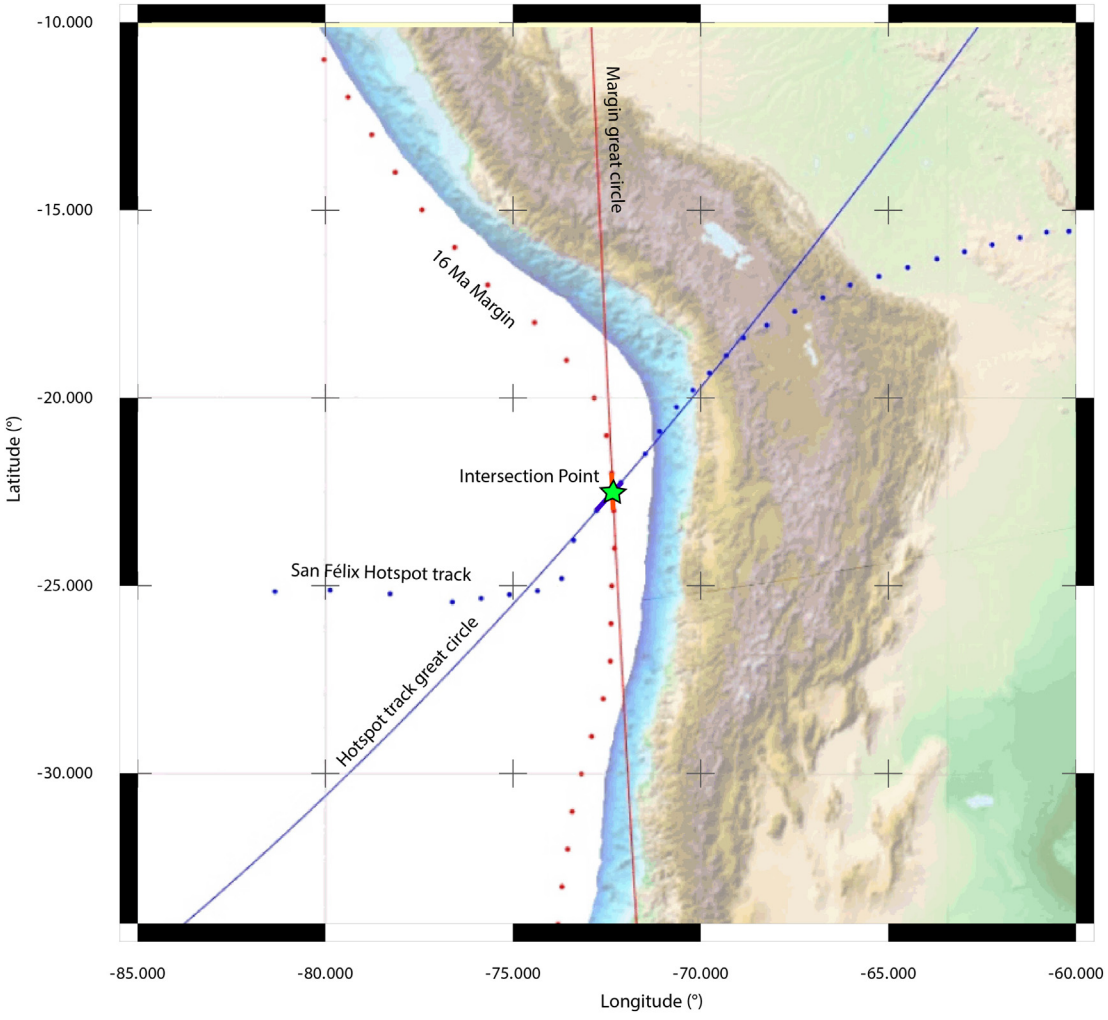

Fig. 4. Intersection point between the western South American margin and San Félix Hotspot track at 16 Ma. The interception point (green star) is defined by the interception between two great circles, one defined by the reconstructed margin segment (highlighted red), and the other defined by the hotspot track segment (highlighted blue).

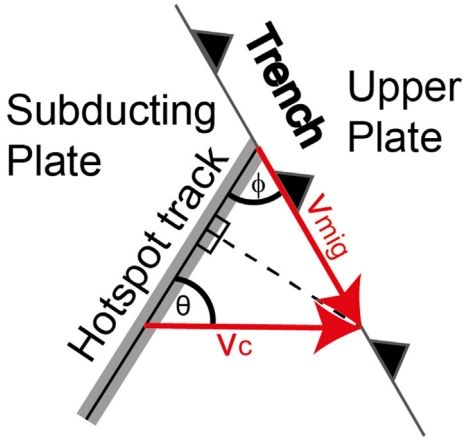

Fig. 5. Geometric relations between the lateral migration velocity Vmig of a bathymetric high parallel to an active plate boundary, the plate convergence velocity Vc, and the orientation of the bathymetric high relative to convergence direction and trench. (Modified from Hampel (2002).)

Figs. S1 and S2). The azimuth and velocity of the convergence vector for each segment in the trench was calculated by the method described in Cox and Hart (1986, Chapter 4). We use the following formula from Hampel (2002):

$$v_{mig} = \frac{v_c \sin\theta}{\sin\varnothing}$$

where v_{mig} is the velocity which a bathymetric high moves along the trench. θ and ∅ are angles defined by the hotspot track orientation with respect to convergence direction and trench, respectively (Fig. 5).

Ages of the subducting seamount for each studied hotspot track since 60 Ma to present were calculated with a time interval of 1 Ma in both models. The age was computed by a linear interpolation within the great circle distance between one step of the motion path and the intersection point with the trench segment (Model 1, Fig. 9; Model 2, Supplementary material Fig. S3). For the visualization and generation of the rotational parameters, we used the software GPlates (Boyden et al., 2011).

4. Results of plate kinematic modeling of the Pacific Ocean

4.1. Easter Seamount Chain, Nazca Ridge and eastern Tuamotu Island Plateau

Several studies (Pilger, 1981, 1984; Steinberger, 2002; Rosenbaum et al., 2005) have considered a common origin between the Easter Seamount Chain and the Tuamotu Plateau at the Easter hotspot. Other observations (Ito and McNutt, 1993; Ito and Lin, 1995) suggest that the Tuamotu Plateau has a near-ridge hotspot origin. There is a lack of geochronological information of this oceanic feature, but an origin of hotspot-ridge interaction should be considered.

Neither Model 1 nor Model 2 does not fit the Pacific branch of the Easter hotspot track to the Tuamotu Plateau. However, there is another parallel bathymetric feature about 360 km northeast of the Tuamotu Plateau, called the eastern Tuamotu Island Plateau (Fig. 1). This feature can be distinguished between the Marquesas FZ and the Austral FZ, and it has also been interpreted as an Easter hotspot plume (Okal and Cazenave, 1985; Steinberger, 2002). The plume erupted when it was located sufficiently close to enable a hotspot-EPR interaction (Okal and Cazenave, 1985; Steinberger, 2002).

Our both models suggest that the eastern Tuamotu Island Plateau formation occurred during Middle Eocene to Early Oligocene, when the Easter Plume was located close to the EPR segment between the Marquesas FZ and Austral FZ (or Mendaña FZ and Nazca FZ in the conjugated features in the Farallon Plate; Figs. 6 and 8A). The EPR segment south of the Austral FZ was about 480 km west of the north Austral FZ EPR segment, specifically at the 27 Ma. Our reconstruction predicts that the Easter Plume "crossed" the Austral FZ, and was placed in the Farallon Plate during that time (Figs. 6 and 8B). In the Nazca Ridge-Easter Seamount Chain elbow zone, the bathymetry does not denote the hotspot track clearly. Therefore, we suggest that the bathymetric elbow was generated during and after the emplacement of Easter Hotspot on the Farallon Plate during the Farallon-Nazca-Cocos break-up. Consequently, Model 1 predicts that the Easter Plume and Salas and Gómez Plume generated the Easter Seamount Chain. Ray et al. (2012) have shown that the age regression of the Easter Seamount Chain fits better with the Salas and Gómez Hotspot location. This can be explained by an age overprinting of the Salas and Gómez plume material over the Easter plume material. Additionally, the azimuth of the line that joins the Salas and Gómez plume with the Easter plume has a similar orientation to the direction of the Nazca Plate absolute velocity vector since the break-up of the Farallon Plate, which support our suggestion of an age overprinting. On the other hand, Kingsley and Schilling (1998) proposed a hotspot located in the vicinity of Salas y Gómez island, which is connected with the EPR via sublithospheric channeling, in a mantle plume source-migrating ridge sink (MPS-MRS) model. Thus, the authors explain the origin of the extensive intraplate neovolcanic seamount chain between Salas y Gómez island and EPR, including the younger age of Easter Island. Seismic finite-frequency tomography (Montelli et al., 2006) shows negative anomalies of shear-wave velocity in the deep mantle, with a radius of 400 km, centered in a location between Easter Island and the Salas and Gómez Island (27°S, 108°W). Based on our reconstruction, we inferred the activity of two plume conducts to explain the Nazca Ridge and the eastern Tuamotu Island Plateau formation, this assumption offers an easier explanation to the elbow intriguing bathymetry. Nevertheless, the mantle setting in the vicinity of the EPR and Easter hotspot is not still well constrained.

4.2. Iquique Ridge and Foundation Chain

The Iquique Ridge has not been dated until now. However, Gutscher et al. (1999) proposed that the Iquique Ridge is the conjugate of the Austral Plateau in the Farallon Plate based on its position between the conjugated Nazca and Austral Fracture Zones, and Resolution and Challenger Fracture Zones (Fig. 1). Nevertheless, the ages obtained by McNutt et al. (1997) of the Austral Plateau's seamounts are about 10 Ma younger than the seafloor below them, suggesting that these seamounts were emplaced far away from the EPR. Therefore, it is unlikely that the Austral Plateau has a conjugated feature in the Farallon-Nazca Plate.

The present Foundation hotspot is located at ~38.8°S, 11.18°W (Mammerickx, 1992; Devey et al., 1997) within the Pacific Plate, about 220 km to the south of the PAC-NAZ-ANT triple junction. The Foundation Chain extends 1800 km in the WNW direction, whereas volcano ages have increased progressively westwards since 21 Ma (O'Connor et al., 1998) (Fig. 2). Local spreading microplate boundaries have migrated systematically toward the Foundation plume for at least the past 21 Ma, which is thought to have led to the formation of the Selkirk microplate (O'Connor et al., 1998).

Model 1 predicts that the Farallon/Nazca Foundation hotspot track coincides with the Iquique Ridge bathymetry. In this perspective, we evaluated the evolution of PAC-FAR-ANT triple junction from Early Oligocene to the Present studied by Tebbens and Cande (1997), to constrain the plate which Foundation hotspot was located before the Farallon break up. Tebbens and Cande (1997) reconstruction predicts that this triple junction was located south of the Chiloé FZ during 25.8 Ma (Chron C8, Fig. 8B), and it jumped at least 300 km northward to the Agassiz FZ before Chron C6o (~20 Ma, Fig. 8C).

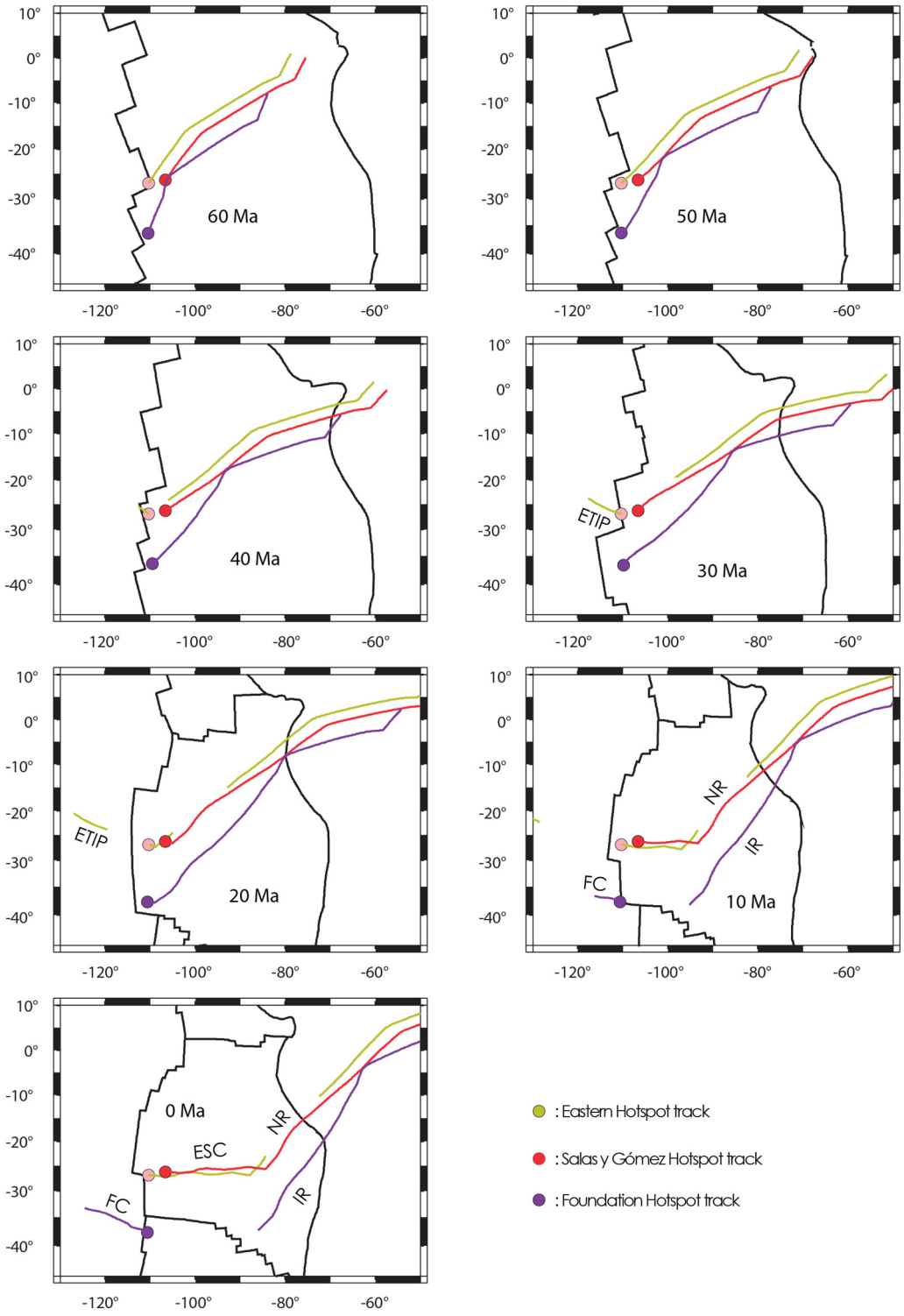

Fig. 6. Plate kinematic reconstruction of the On-Ridge hotspot tracks from 60 Ma to present. Predicted path for the Nazca Ridge (NR) from Salas y Gomez hotspot, Easter Seamount Chain (ESC) and eastern Tuamotu Island Plateau (ETIP) from Easter hotspot, and Iquique Ridge (IR) and Foundation Chain (FC) from Foundation hotspot since Paleocene time. The margin of South America moves westward, while the hot spot locations remains stationary, based on Model 1.

This reconfiguration of the FAR-PAC-ANT plate boundary implies that the Selkirk microplate was transferred to the Pacific Plate, and migrated about 350 km westward of the ridge between the Mocha FZ and the Resolution FZ. This process was relatively synchronized with the Farallon plate break-up, and it was also part of a greater re-accommodation process in the southeast Pacific at that time. Regarding Tebbens and Cande (1997) reconstruction, Model 1 predicts that the Foundation hotspot passes the Challenger (Resolution) FZ from the north to south at ~25 Ma (Fig. 8B), implying that the overlying plate transitioned from the Farallon plate to the Pacific plate. Furthermore, this process caused the cessation of volcano construction at the Iquique Ridge seamounts track, and thereby initiated volcanism at the Foundation Chain (Figs. 6 and 8C). This hypothesis is temporally consistent with the oldest and the westernmost dated sample found in the

Foundation Chain (Seamount 1a in O'Connor et al., 1998), and the occurrence of Foundation Chain seamounts overlying the Selkirk microplate seafloor (Fig. 8).

4.3. Juan Fernández Ridge, Copiapó Ridge and Taltal Ridge

At present, the Juan Fernández, Copiapó and Taltal Ridges are three parallel ridges with near E-W strike that subduct at 32.5°S, 27.3°S and 25.2°S, respectively. During their formation, both models predicts that distance between those ridge bathymetries diminish when the Nazca Plate absolute direction is oblique with respect to the N10 W line between Juan Fernandez and San Félix hotspots (Fig. 7, 60–30 Ma), This line is similar with respect to the margin strike, and the parallel bathymetry (similar strake) of the ridges separated when the Nazca Plate absolute direction became orthogonal respect to the N10W line (Fig. 7, 10–0 Ma).

5. Discussion

Our calculations show that there are similar kinematic patterns between the elements of the on-ridge and also the off-ridge hotspot tracks (Fig. 9). We consider that this phenomenon is merely due to the position of the plumes and their plate kinematic frameworks. Nevertheless, the collision of the oceanic ridges plays an important role on the processes of mountain building, magmatism, and metallogenesis. Some of these implications are discussed in the following sections.

5.1. Off-ridge Hotspots tracks migration

The Taltal, Copiapó and the Juan Fernández Ridges, between 60 and 47.9 Ma (C21n) were subducting with a slow, but constant southward migration velocity (20 to 30 km/Ma). These ridges migrated about 300 km southward from south Peru (17°S), to the Bolivian orocline axis (~20°S) during the same period (Fig. 7). At ~40 Ma, the Taltal

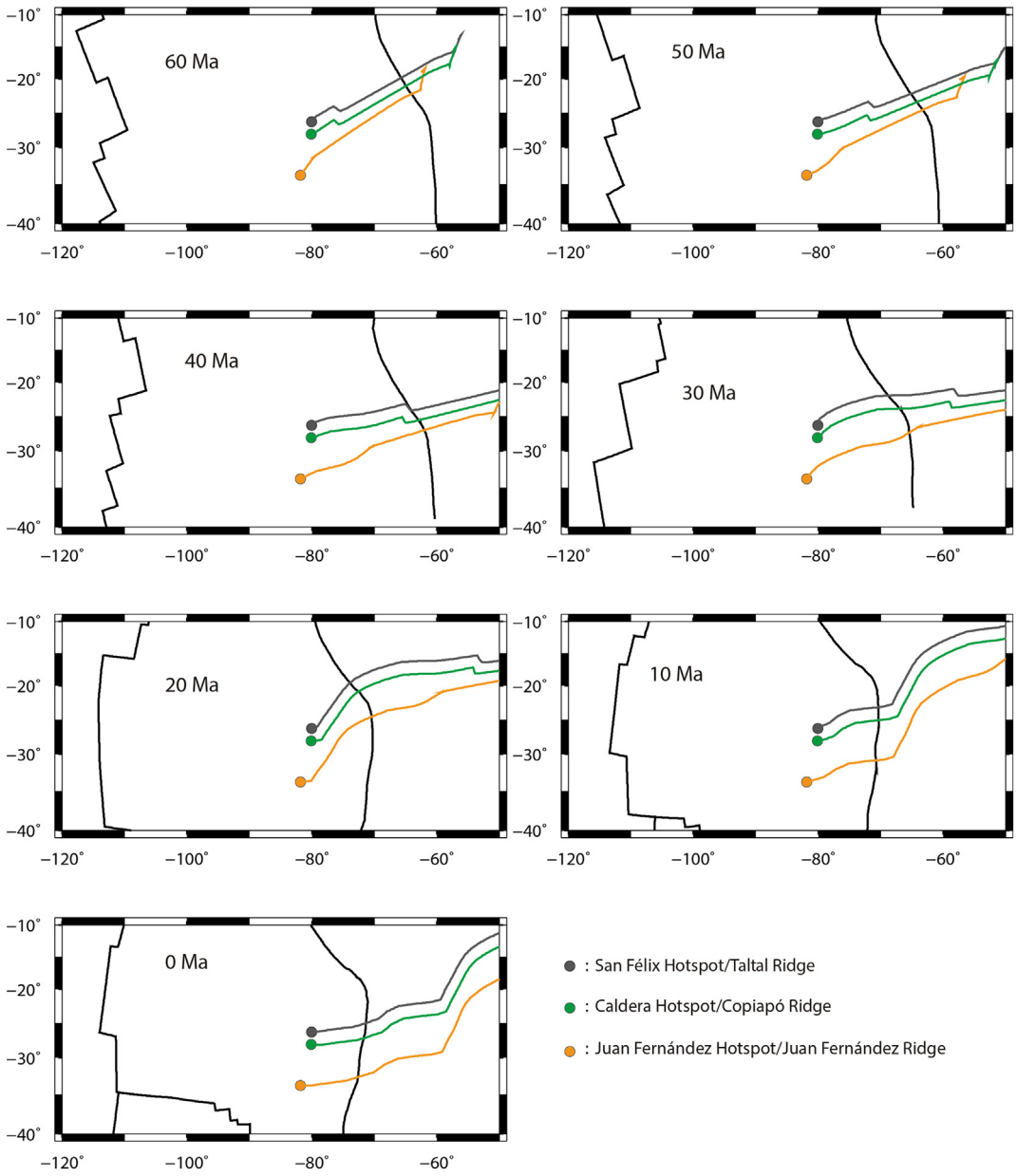

Fig. 7. Plate kinematic reconstruction of the Off-Ridge hotspot tracks from 60 Ma to present. Predicted path for the Juan Fernández, Taltal, and Caldera hotspot tracks since Paleocene time. The margin of South America moves westward, while the hotspot locations remain stationary, based on Model 1.

Ridge and Copiapó Ridge had a steep and short northward migration (Figs. 7 and 9) associated with the subduction of the hotspot track segments built up between 83 and 73.62 Ma (C34n-C33n) when Model 1 predicts a period of slow and northward Nazca Plate absolute velocity, generating an abrupt, but relatively short (about 150 km) change in the azimuth of these features. Between 40 and 27 Ma (C18r-C9n), these hotspot tracks' migration acquired a quasi-stationary behavior, mainly because the azimuths of these hotspot tracks were similar to the convergence velocity azimuth (Figs. 7 and 9).

A period of flat-slab subduction was recorded in southern Peru and northern Bolivia between 14°S and 20°S (James and Sacks, 1999). This flat slab was inferred based on a rapid cessation of the magmatic arc between 45 and 35 Ma, widespread deformation and crustal thickening in the Eastern Cordillera, and the lack of known igneous rocks of the same age in this segment (Ramos and Folguera, 2009). These processes are explained by a decrease in the angle of subduction that became subhorizontal at about 35 Ma and lasted until ~25 Ma (Ramos and Folguera, 2009). Counterclockwise block rotations in southern Peru (Roperch et al., 2006, 2011) and clockwise block rotations in northern Chile (Abels and Bischoff, 1999; Arriagada et al., 2008) have been recorded. Arriagada et al. (2008) predicted that the major block rotations took place between 45 and 15 Ma. Scheuber and Reutter (1992) proposed a period of strong orogen-normal shortening with a slightly dextral parallel strike-slip component in the central Andes (21–25°S) between 40 and 35 Ma. Additionally, they proposed back arc folding and thrust belt deformation. These features configure a scenario of a flat slab according to tectonic considerations of Gutscher et al. (2000) with a slightly dextral convergence vector in the central Andes. James and Sacks (1999) proposed a flattering slab during this period, with clockwise block rotations. Both models considered in this study predict an orthogonal convergence component between 90 and 100 km/Ma with a slightly dextral convergence vector (0–20°) in northern Chile. Model 1 and Model 2 also suggests a strong sinistral convergence vector (30–50°) in southern Peru (10°–20°S), which occurred between 47 and 27 Ma (Figs. 10C, D, S1, S2).

In addition, Model 1 and Model 2 predict that the Juan Fernández Ridge was subducting at 20–25°S (considering South America fixed) between 40 and 20 Ma. We propose that the Juan Fernández, Copiapó and Taltal Ridges subduction contribute partially to the slab flattening, generating a strong orogen normal shortening, back arc folding, and thrust belt deformation. Furthermore, due to an increase of interplate coupling left by the flattening slab, the parallel trench component of the convergence velocity enables strain partitioning (Pinet and Cobbold, 1992; Pubellier and Cobbold, 1996; Chemenda et al., 2000) which is evident by dextral orogen parallel strike-slip, clockwise block rotations in northern Chile and counterclockwise block rotations in southern Peru since Late Eocene to Late Oligocene epochs.

In the Late Oligocene epoch, 27.03–22.75 Ma (C9n-C6Bn.1r), Model 1 predicts an increase of the convergence velocity from ~120 to ~140 mm/yr, and its azimuth turned toward the NE (Fig. 10). This change in the Farallon Plate motion generated a northward migration of these off-ridge hotspot tracks, about 64–70 km/Ma in Model 1 (Figs. 7 and 9).

A period of significant crustal shortening in the Altiplano and Eastern Cordillera occurred primarily between ~40 and 30 Ma (Lamb and Hoke, 1997; Lamb et al., 1997; McQuarrie, 2002). This period coincides temporally and spatially with the formation of the Bolivian Orocline and the subduction of three ridges formed at the San Félix, Caldera and Juan Fernández hotspots for both models. Our seamount age calculations predict that the San Felix and Caldera hotspot tracks were subducting as surrounding younger and then more buoyant oceanic crust than the Juan Fernandez hotspot track (Fig. 9A). Gutscher et al. (2000) and Huangfu et al. (2016) proposed that young (<50 Ma) thickened oceanic crust is more favorable to generate a flat slab segment.

A widespread volcano-sedimentary extensional basin was setting in southern Andes between 33 and 45°S during middle Oligocene to early Miocene (e.g. Jordan et al., 2001; Charrier et al., 2005). In addition, Hoke and Lamb (2007) and Kay et al. (2008) proposed back-arc bimodal magmatism in the Altiplano and western margin of the Eastern Cordillera as evidence for an already thin lithospheric mantle beneath the Altiplano since ~25 Ma, this period also corresponds to the onset of shortening in the Eastern Cordillera of the Central Andes (e.g., Lamb and Hoke, 1997; Oncken et al., 2006; Roperch et al., 2006) and the absence of magmatic activity between 22 and 24°S (Kay et al., 2008). This tectonic segmentation is temporally coincident with the highest convergence rate during the Cenozoic Era (Fig. 10). Flat slab was only proposed in Central Andes (James and Sacks, 1999; Kay et al., 1999), where our both hotspot track models predict ridge-trench collision until early Miocene (Fig. 9A).

The bathymetric relief azimuth generated during late Oligocene-early Miocene was directed toward the NE, and it was parallel and synchronous with the present-day Nazca or Iquique Ridge (Fig. 1B). However, three NE ridges, ~1000 km long, formed at the San Félix, Caldera and Juan Fernández hotspots and began subducting the following 7 Ma during Early Miocene until ~15 Ma (Model 1). The subduction of these three NE ridges is coincident with the change in convergence azimuth toward the Eastern direction due the break-up of the Farallon plate (Figs. 7 and 10). This process generated a rapid southward migration from the Central Andes to the near present-day latitude of subduction (Taltal Ridge: 29.25°S, Copiapó Ridge: 27.4°S and Juan Fernández Ridge: 32.8°S) with accelerated southward migration velocities from 60 to 300 km/Ma during the Early Miocene epoch (~22.7–16 Ma, Fig. 9).

Kay and Abbruzzi (1996) proposed a Miocene flat slab (18–12 Ma) in the La Puna zone. This relatively short-lived flat slab could have been driven by the rapid southward migration of the Juan Fernández, Copiapó and Taltal Ridges during this period (Fig. 9). Muñoz-Sáez et al. (2014) proposed that the Aconcagua fold-thrust belt initiated in the Middle Miocene, ~16 Ma. This process entails a foreland migration of crustal deformation that could be explained by slab flattening (Jordan et al., 1983; Smalley et al., 1993). Peneplains in the Easter Coastal and western Principal Cordilleras would have corresponded to the same geomorphological surface prior to the rapid and high magnitude regional uplift of the central Chilean Andes during Late Miocene (Farías et al., 2008). Arriagada et al. (2013) proposed that since Late Miocene to present, about a 15° clockwise block rotation occurred in the Andes at ~25–35°S, which continues to generate the Maipo Orocline (Arriagada et al., 2013). Our both models predict that Juan Fernández Ridge took place at 25–35°S margin ~15 Ma (Fig. 11), and that this feature has remained in a relatively quasi-stationary state of subduction until now (Figs. 7 and 9).

This work suggests that the subduction of the analyzed off-ridge hotspot tracks was a first order factor in building the Bolivian and Maipo Orocline (Martinod et al., 2010; Bello-González, 2015). This process was caused by slab flattening which is induced by the buoyancy of subducting hotspot tracks, and evident by the flat slab/normal slab along arc propagation observed by James and Sacks (1999).

5.2. On-ridge hotspots tracks migration

Our hypothesis suggests that the Foundation hotspot was located below the Farallon Plate before 25 Ma where the Iquique Ridge was formed. When the Foundation hotspot intercepted the Challenger FZ, it changed to the Pacific Plate, then, the Foundation hotspot stopped building the Iquique Ridge, and it began generating the Foundation Chain (Model 1, Figs. 6 and 8). This hypothesis is also consistent with the extension of the Foundation Chain from the failed rift of the Selkirk microplate, located 600 km to the west, which could have occurred 4 Ma after the rapid Selkirk microplate formation and extinction. Dating the seamount located at 35.1°S and 81.3°W, would provide important constraints to rule out our proposed hypothesis. This seamount could be the youngest one of the Iquique Ridge before the jump of the

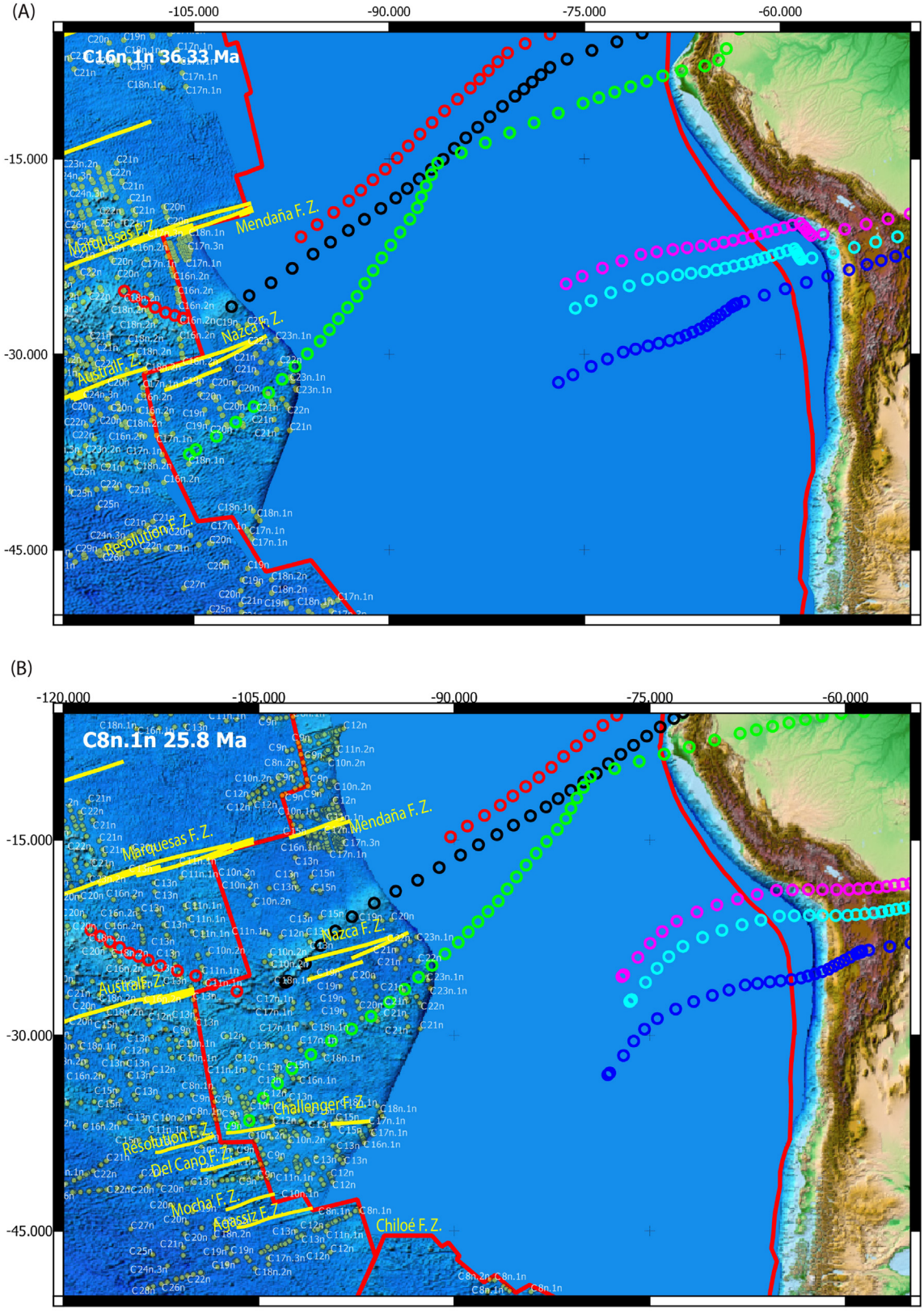

Fig. 8. (A) Tectonic reconstruction at 36.33 Ma of the Model 1 Nazca hotspot trends, during this time, Easter Hotspot plume was located below the Pacific Plate, and it was building the eastern Tuamotu Island Plateau. (B) Tectonic reconstruction at 25.8 Ma of the Nazca hotspot trends, at that time Nazca FZ have passed above the Easter Hotspot plume, and it began building the Easter Seamount Chain. (C) Tectonic reconstruction at 21.13 Ma of the Nazca hotspot trends, at this moment Selkirk Microplate is accreted to the Pacific Plate, and Challenger FZ have passed above the Foundation Hotspot plume, changing the plate of this plume from Farallon Plate to Pacific Plate. The 600 km west extension of the Foundation Chain from the Selkirk microplate has been generated. Reconstructions consider Nazca Hotspot frame fixed.

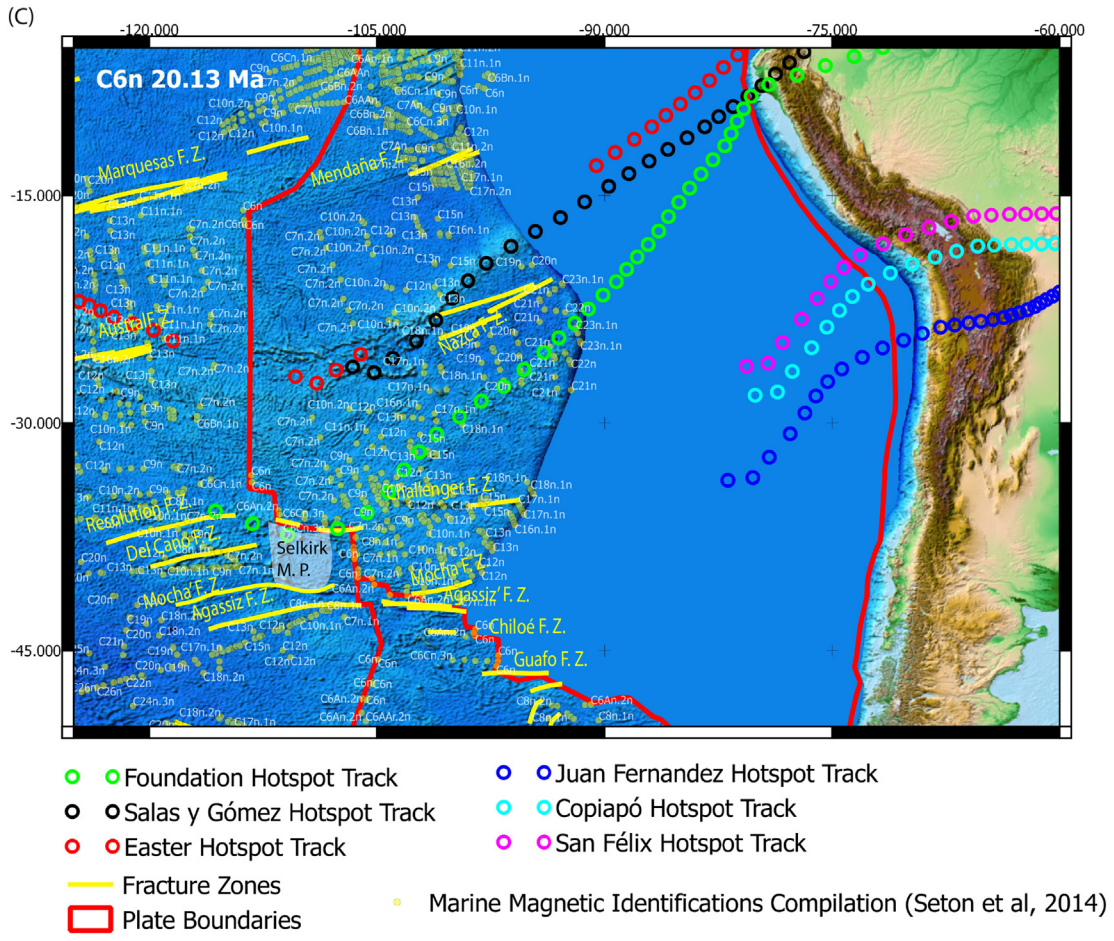

Fig. 8 (*continued*).

Foundation hotspot to the Pacific plate, and it should be slightly older than the O'Connor et al.'s (1998) Seamount 1a (21.2 ± 0.1 Ma).

Between the Latest Eocene to Earliest Miocene, Easter, Salas y Gómez and Foundation hotspot tracks were subducting off the coast of Ecuador (Figs. 6 and 9A). At 40 to 30 Ma, these oceanic features remained quasi-stationary (stationary ridge subduction). In contrast, during the middle to late Oligocene (30–23 Ma), these ridges continued to subduct at Ecuadorian latitude, but with an oscillating migration velocity due to a change in the convergence vector at C9n (27.03 Ma) (Figs. 6 and 9B).

The Oligocene period is represented by a widespread hiatus in the Ecuadorian coastal region (Benitez et al., 1993; Benitez, 1995; Luzieux, 2007), whereas in the Oriente Basin, Oligocene sediments of the Orteguaza Formation lie above truncated beds of the Tiyuyacu Formation (e.g. Balkwill et al., 1995). This unconformity may be related to a regional tectonic event in the adjacent western and eastern cordilleras as well as forearc regions (Vallejo, 2007). Spikings et al. (2000, 2001, 2005) discovered elevated exhumation rates in the Eastern Cordillera during 43–30 Ma.

Kerr et al. (2002) defined the Naranjal Block that is located north of the Western Cordillera in the Andes of Ecuador. The Naranjal unit is a volcanic sequence consisting of andesitic and basaltic tholeiitic rocks in the eastern part, and oceanic plateau affinity in the southwest. The same study concluded that the accretion of the Naranjal Block onto the continental margin took place during the Eocene epoch. Radiolarian fauna is present in mudstones intercalated in pillow lavas of island arc affinity (Boland et al., 2000; Kerr et al., 2002) located in the southwestern part of the sequence. Therefore, the Naranjal Block basement is an oceanic plateau possibly older than the late Campanian (Vallejo, 2007). Thus, the oceanic Plateau should have been accreted onto the continental margin during the Eocene epoch (Kerr et al., 2002). This is consistent with the age of the hotspot track segment that was subducting during the Eocene in the Naranjal Block at present day latitude (Fig. 9A). Our both reconstruction models suggest that the Easter and the Salas and Gómez plume material could have formed the Naranjal block basement. To reach a conclusion, geochemical and petrological studies are necessary.

During the Miocene epoch to the present, the migration of the group of on-ridge seamount tracks follows an oscillating southward trajectory (Figs. 6 and 9). Between 20 and 15 Ma (chron C5Bn.2n), the migrating velocity ranged from 100 to 200 km/Ma due to (1) the angle difference between the NE trend of the ridges defined during the Late Cretaceous by the on-ridge plumes, (2) the E-W convergence velocity vector azimuth, and (3) the NW trench's azimuth which corresponds to the Peruvian Andes. During 14 to 11 Ma, the subduction of these off-ridges hotspot tracks was quasi-stationary in the central Peruvian Andes. A similar quasi-stationary regime took place from 5 to 3 Ma, and the Easter and Salas and Gómez hotspot tracks subducted beneath the south Peruvian Andes while the Foundation hotspot track (Iquique Ridge) subducted beneath the Arica bend zone. These two quasi-stationary regime periods were associated with a ridge azimuth parallel to the convergence velocity vector azimuth, and they could be related to the Peruvian flat slab formation since 11 Ma to present (Pilger, 1984; Gutscher et al., 1999; Hampel, 2002; Ramos and Folguera, 2009).

This work predicts that the subducting seamount's age has been decreasing over the last 60 Ma (Fig. 9A). The difference in the age of the seamounts when they subduct is dictated by the velocity of the South

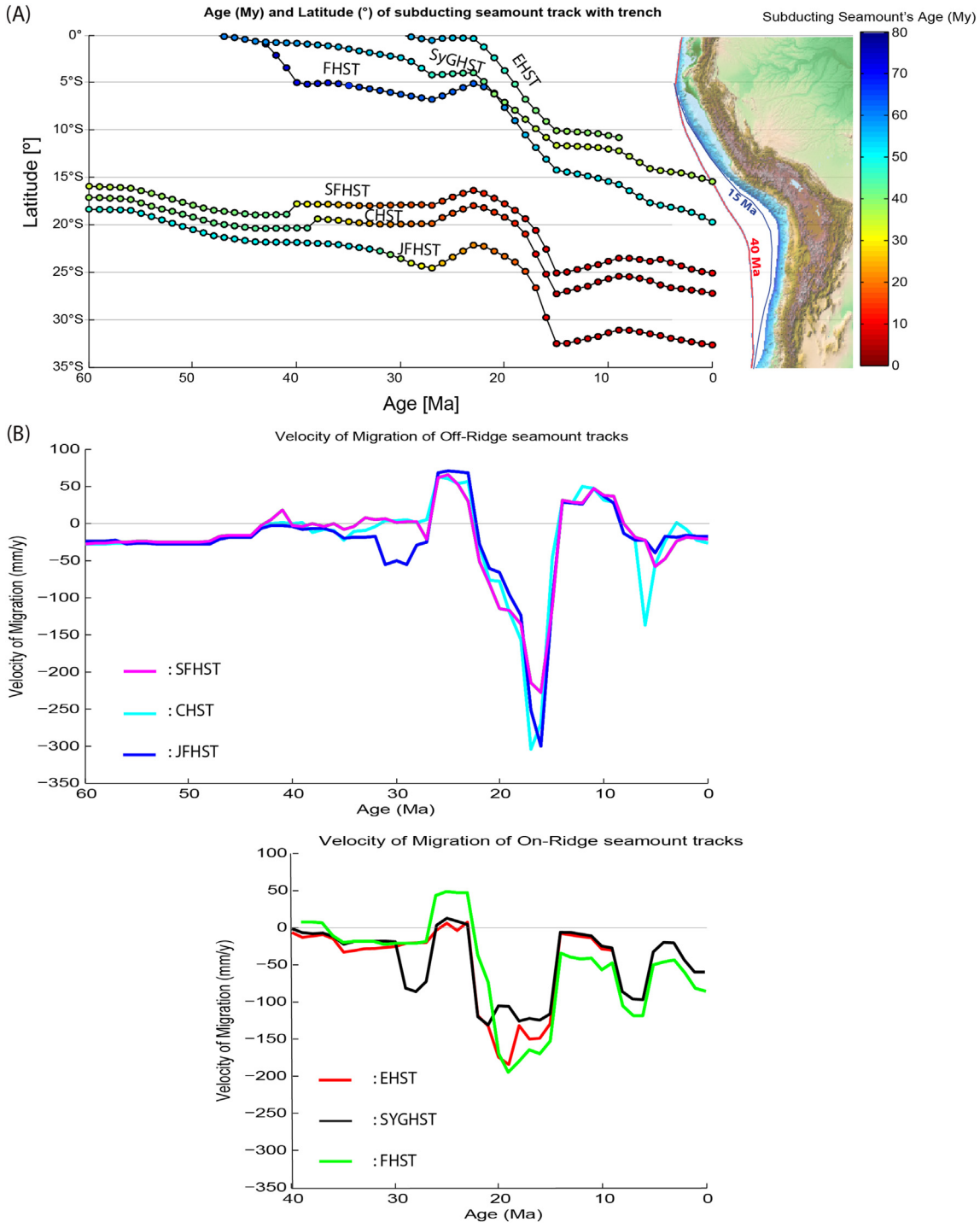

Fig. 9. (A) Intersection point latitude was calculated between the trench axis and the hotspot tracks from Model 1. Colors represent the predicted seamount's age at the subduction time. (B) Velocity of migration of the hotspot tracks move along the western South American margin. The red, black and green curves correspond to the on-ridges hotspot tracks (EHST: Easter, SyGHST: Salas y Gómez, and FHST: Foundation hotspot tracks respectively), the magenta, cyan and blue curves represent to the off-ridges hotspot tracks (SFHST: San Felix, CHST: Caldera and JFHST: Juan Fernández hotspot tracks respectively). Reconstruction considers South America fixed.

American and Nazca plates with respect to the Nazca hotspots. The absolute westward velocity of South America last 80 Ma have been related to the whole mantle convection rate, which is enhanced by lower mantle penetration of the Farallon/Nazca slab (Schellart, 2017; Faccenna et al., 2017). Silver et al. (1998) proposed that the South American plate is currently moving faster relative to the hotspots than at any time in the last 80 Ma before the velocity increase occurred between 30 and 25 Ma. This event coincides with an increase in convergence velocity between the Nazca and South American plates proposed by Somoza (1998) and our reconstruction (Fig. 10).

5.3. Model 1 and Model 2 comparison

We compare both interception points models, and we contrasted them with the trench advance associated to the Bolivian Orocline formation (Fig. 11). We consider the heterogeneity in trench motion

with respect to South America craton as rate of lithospheric continental shortening. The off-ridge collision points shown by Model 1 coincide apparently with the highest trench advance rate along the margin during 40–20 Ma. Model 2 shows a weaker correlation between hotspot track-trench collision points and highest trench advance rates, However, off-ridge intersection point of this model are mostly located integrally between 15°S and 30°S (40–15 Ma), where Bolivian Orocline was generating.

During 15 Ma to present, we observe an increase in the trench advance rate in north and south segments of the margin, this is also consistent with Nazca Ridge and Juan Fernandez Ridge arriving in the northern and southern margin segment respectively.

Both models provided can be used to explain the continental deformation based on flat slab occurrence by positive buoyancy of an anomalously thick oceanic crust (Gutscher et al., 2000) that trigger and maintain a flat slab underlain by the overpressured sub-slab mantle (Schepers et al., 2017).

5.4. Hotspot location and plate reorganizations

The reconfiguration of plate boundaries during plate reorganization events can be strongly influenced by hotspot location based on our observations. This is likely due to a weakening in the oceanic lithosphere associated with a thermal anomaly related to upwelling plumes. That

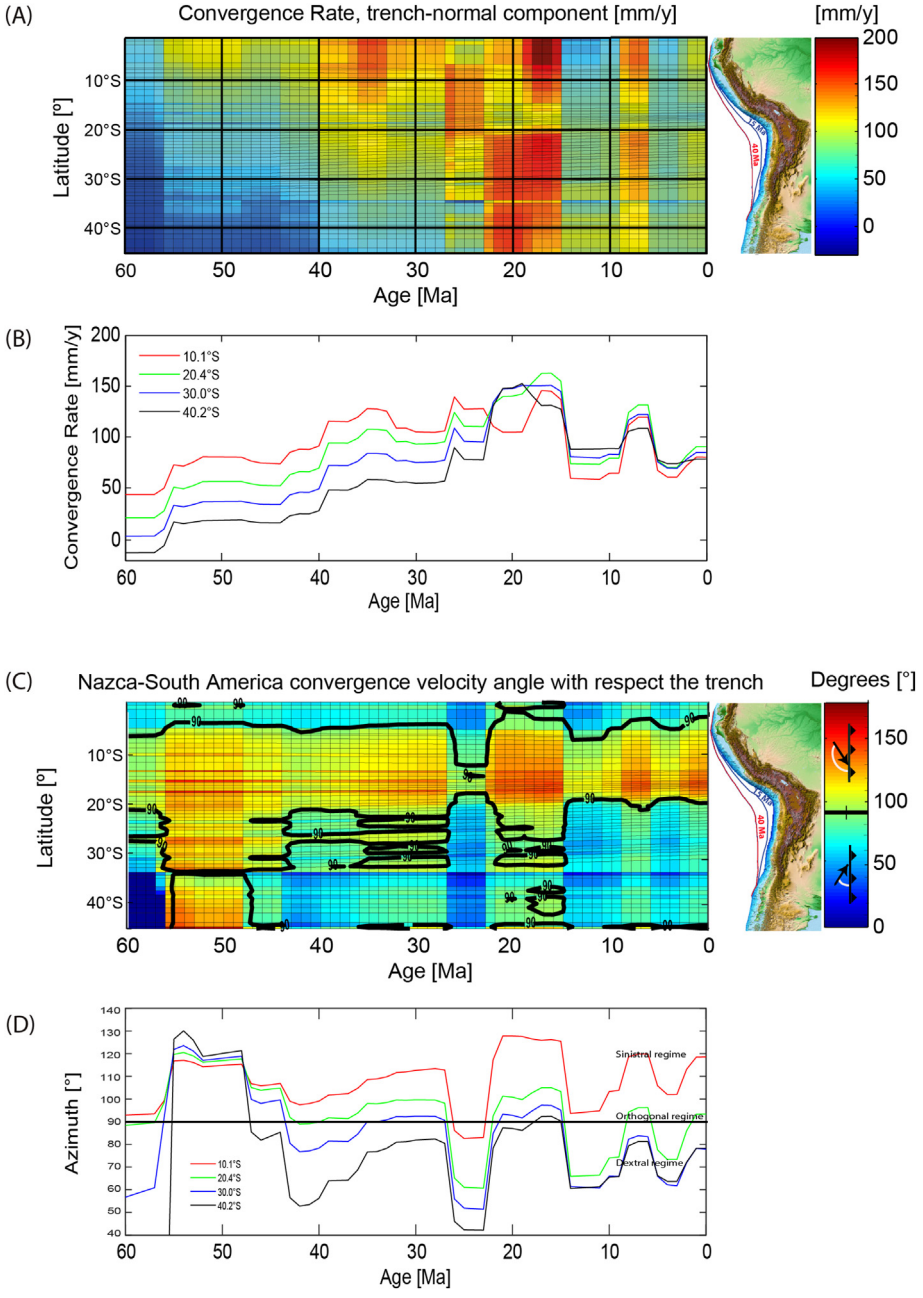

Fig. 10. Model 1: (A) Nazca-South America orthogonal convergence rate in the trench, based on the relative plate motions from poles of rotations shown in Table 3 and reconstructed margin from Bolivian and Maipo Oroclines (Arriagada et al., 2008). (B) The red, green, blue and black curves correspond to the extracted convergence rate curves from the grid shown in (A) at 10.1°S, 20.4°S, 30°S, and 40.2°S, respectively. (C) Nazca-South America convergence velocity angle with respect the trench based on the relative plate motions from poles of rotations shown in Table 3 and reconstructed margin from Bolivian and Maipo Oroclines, reddish colors represent sinistral regimes, the wide black line depicts trench-normal convergence, and blueish colors represent dextral regimes. (D) The red, green, blue and black curves correspond to the convergence velocity angle with respect the trench extracted from the grid shown in (C) at 10°S, 20°S, 30°S, and 40°S, respectively. Reconstruction considers South America fixed.

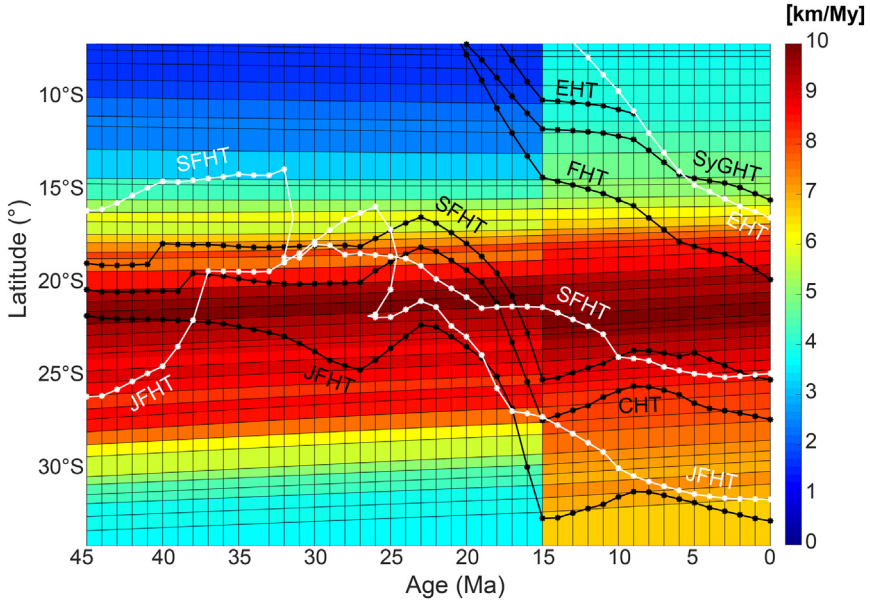

Fig. 11. Intersection point latitude was calculated between the trench axis and the hotspot tracks from Model 1 (in black) and Model 2 (in white). Colors represent the trench advance rate associated with the Bolivian Orocline restoration (Arriagada et al., 2008) South America is anchorage. SFHT: San Felix Hotspot Track, CHT: Caldera Hotspot Track, JFHT: Juan Fernández Hotspot Track, EHT: Easter Hotspot Track, SyGHT: Salas y Gómez Hotspot Track, and FHT: Foundation Hotspot Track.

a relevant factor in the formation of the Selkirk microplate would be a weakening in the Farallon plate in the place where the Foundation hotspot was located. The Selkirk microplate formation, extinction, and accretion to the Pacific Plate, implied a jump of the PAC-ANT-FAR triple junction, at least 340 km northward from the Mocha FZ to the Challenger FZ. This jump of the PAC-ANT-FAR triple junction resulted in a 350 km migration westward of the EPR between the Mocha FZ and the Resolution FZ (Fig. 8). Similar processes of lithospheric weakening and breaking plate occurred simultaneously in the Farallon plate break-up, possibly driven by the Galapagos hotspot plume (Barckhausen et al., 2008; Hey, 1977; Lonsdale, 2005). Another case was the break up and reconfiguration of the Phoenix Plate at ~123 Ma, when the building and fragmentation of the Ontong Java Nui Plateau resulted from a plume-Tiple Junction interaction (Larson et al., 2002; Viso et al., 2005). Chandler et al. (2012) associated the Louisville hotspot with the Ontong Java Nui generation. Therefore, the position of the hotspots could be a first order factor of the reconfiguration of plate boundaries during plate reorganization events.

6. Conclusions

On-ridge hotspots interact with active spreading centers and fracture zones. These hotspots are susceptible to alter the tectonic plate where they generate seamount and aseismic ridges. This process could happen when a segment of the spreading center intercepts a plume, or a plume is located between two segments of a mid-ocean ridge separated by a fracture zone, which allows the plume to intercept the fracture zone. This interaction could result in the interruption of a seamount chain formation, and the beginning of a seamount chain in the conjugated plate. We suggest that the eastern Tuamotu Island Plateau was generated by the Easter hotspot at 48–27 Ma. In this period, the Easter hotspot was beneath the Pacific Plate west of the EPR segment between the Marquesas FZ and the Austral FZ. During the interception between the Easter hotspot and the Austral FZ, the Easter Seamount Chain became active on the Farallon Plate. Similarly, the Foundation hotspot was located below the Farallon Plate before 25 Ma, and was building the Iquique Ridge. During the interception of the Iquique Ridge by the Challenger FZ, the Foundation hotspot transferred to the Pacific Plate, at which point it stopped building the Iquique Ridge and began generating the Foundation Chain.

The Selkirk microplate formation and extinction in addition to the PAC-FAR-ANT Triple Junction northward jump at 23 Ma, could have been affected by the thermal anomaly of the Foundation hotspot. Furthermore, the Farallon Plate break up at ~22.7 Ma in the Nazca and Cocos plates which occurred above the Galapagos hotspot, and the Ontong Java Nui fragmentation have both been determined as a hotspot-ridge interaction. These examples are evidences that the position of hotspots could be a first order factor of the reconfiguration of plate boundaries during plate reorganization events. This is likely due to a weakening in the oceanic lithosphere associated with a thermal anomaly related to upwelling plumes.

Between the Late Eocene to Early Miocene epochs, three off-ridge hotspot tracks maintained quasi-stationary subduction where trench advance rate related to the Bolivian Orocline was highest. Furthermore, the trench-parallel component of the convergence velocity could lead strain partitioning due to an increase of interplate coupling triggered by the flattening slab. This strain partitioned is evidenced by dextral orogen parallel strike-slip, clockwise block rotations in northern Chile and counterclockwise block rotations in southern Peru since Late Eocene. La Puna short live flat slab (18–12 Ma) coincides with the period of rapid southward migration of the off-ridge hotspot tracks. In addition, clockwise rotation of the central Chilean Andes during the Late Miocene to present generates the Maipo Orocline, which coincides spatially and temporally with a quasi-stationary subduction of the Juan Fernández Ridge at the same latitude. Apparently, a quasi-stationary, aseismic ridge subduction state drives slab flattering, oroclinal rotations, crustal thickening, foreland deformation migration, and volcanic quiescence.

Our reconstruction suggests that the Naranjal block basement, in north Ecuador could have been originated in the Easter and Salas and Gómez hotspots, geochemical and petrological studies are necessary to support or discard this hypothesis.

Comparing the accreting behavior of the northern Andes and the subducting behavior of the central Andes is an interesting approach to understand the tectonic factors effecting the high bathymetric relief and trench interaction in these areas.

Acknowledgments

Eduardo Contreras-Reyes acknowledges the support of the Chilean National Science Foundation (FONDECYT) project 1170009 and the

support of Programa de Investigaciòn Asociativa: ANILLOS DE INVESTIGACION EN CIENCIA Y TECNOLOGIA, CONICYT, grant ACT172002, project title "*The interplay between subduction processes and natural disasters in Chile*.". We are greatly grateful for the support provided by Mikenna Martin for the English editing. We are very thankful to Pierrick Roperch, for shearing their orocline block rotation file, and Pavel Doubrovine, for his constructive suggestions. We thank the comments and suggestions of Douwe van Hinsbergen and another anonymous reviewer, which improved substantially the original manuscript.

Appendix A. Supplementary data

Supplementary data to this article can be found online at https://doi.org/10.1016/j.gr.2018.07.008.

References

Abels, A., Bischoff, L., 1999. Clockwise block rotations in northern Chile: indications for a large-scale domino mechanism during the middle-late Eocene. Geology 27 (8), 751–754.

Álvarez, O., Gimenez, M., Folguera, A., Spagnotto, S., Bustos, E., Baez, W., Braitenberg, C., 2015. New evidence about the subduction of the Copiapó ridge beneath South America, and its connection with the Chilean-Pampean flat slab, tracked by satellite GOCE and EGM2008 models. Journal of Geodynamics 91, 65–88. https://doi.org/10.1016/j.jog.2015.08.002.

Amante, C., Eakins, B.W., 2009. ETOPO1 1 arc-minute Global Relief Model: Procedures, Data Sources and Analysis. NOAA https://doi.org/10.7289/V5C8276M.

Anderson, M., Alvarado, P., Zandt, G., Beck, S., 2007. Geometry and brittle deformation of the subducting Nazca Plate, Central Chile and Argentina. Geophysical Journal International 171, 419–434.

Araya, P., 2015. Efectos de la subducción de la dorsal de Juan Fernández en la geoquímica del volcanismo de 18° a 33°S. Memoria de Título, Dep. de Geología, FCFM, U. de Chile.

Arriagada, C., Roperch, P., Mpodozis, C., Cobbold, P., 2008. Paleogene building of the Bolivian Orocline: tectonic restoration of the central Andes in 2-D map view. Tectonics 27, TC6014. https://doi.org/10.1029/2008TC002269.

Arriagada, C., Ferrando, R., Córdova, L., Morata, D., Roperch, P., 2013. The Maipo Orocline: a first scale structural feature in the Miocene to Recent geodynamic evolution in the central Chilean Andes. Andean Geology 40 (3), 419–437. https://doi.org/10.5027/andgeoV40n2-a02.

Astudillo, V., 2014. Geomorfología y evolución geológica de la Isla Robinson Crusoe, Archipiélago Juan Fernández. Memoria de Título, Dep. de Geología, FCFM, U. de Chile.

Atwater, T., 1989. Magnetic anomalies in the North Pacific. Geology of North America. Geological Society of America.

Balkwill, H.R., Rodriguez, G., Paredes, F.I., Almeida, J.P., 1995. Northern part of Oriente Basin, Ecuador: reflexion seismic expression of structures. In: Tankard, A.J., Suarez, S., Welsink, H.J. (Eds.), Petroleum Basins of South America. American Association of Petroleum Geologists, Memoir vol. 62, pp. 559–571.

Ballance, P.F., Scholl, D.W., Vallier, T.L., Stevenson, A.J., Ryan, H., Herzer, R.H., 1989. Subduction of a Late Cretaceous seamount of the Louisville Ridge at the Tonga Trench: a model of normal and accelerated tectonic erosion. Tectonics 8 (5), 953–962. https://doi.org/10.1029/TC008i005p00953.

Barckhausen, U., Ranero, C., Huene, R., Cande, S., Roeser, H., 2001. Revised tectonic boundaries in the Cocos plate off Costa Rica: implications for the segmentation of the convergent margin and for plate tectonic models. Journal of Geophysical Research. Solid Earth 106 (B9), 19207–19220.

Barckhausen, U., Ranero, C., Cande, S., Engels, M., Weinrebe, W., 2008. Birth of an intraoceanic spreading center. Geology 36 (10), 767–770.

Bello-González, J.P., 2015. Reconstrucción tectónica de la cuenca del Pacífico durante el Cretácico Tardío y Cenozoico, implicancias en el desarrollo de los Andes. Memoria de Título, Dep. de Geología, FCFM, U. de Chile.

Benitez, S., 1995. Évolution géodynamique de la province côtière sud-équatorienne au Crétacé supérieur-Tertiaire. Université Joseph-Fourier - Grenoble I (Applied geology, 1995, French).

Benitez, S., Jaillard, E., Ordoñez, M., Jimenez, N., Berrones, G., 1993. Late Cretaceous to Eocene tectonic-sedimentary evolution of southern coastal Ecuador. Geodynamic implications. Second ISAG, Oxford (UK), 21–23/9/1993.

Bernard, A., Munschy, M., Rotstein, Y., Sauter, D., 2005. Refined spreading history at the Southwest Indian Ridge for the last 96 Ma, with the aid of satellite gravity data. Geophysical Journal International 162 (3), 765–778.

Boland, M.P., Pilatasig, L.F., Ibandango, C.E., McCourt, W.J., Aspden, J.A., Hughes, R.A., Beate, B., 2000. Geology of the Western Cordillera between 0°–1°N. Proyecto de Desarrollo Minero y Control Ambiental, Programa de Informacion cartografica y Geológica, Informe No. 10. CODIGEM-BGS, Quito, Ecuador (72 pp.).

Boyden, J., Müller, R., Gurnis, M., Torsvik, T., Clark, J., Turner, M., Ivey-Law, G., Watson, R., Cannon, J., 2011. Next generation plate-tectonic reconstructions using Gplates. In: Keller, G.R., Baru, C. (Eds.), Geoinformatics: Cyberinfrastructure for the Solid Earth Sciences. Cambridge University Press, Cambridge, U. K., pp. 95–114 https://doi.org/10.1017/CBO9780511976308.008.

Cande, S.C., Stock, J.M., 2004. Cenozoic reconstructions of the Australia-New Zealand-South Pacific sector of Antarctica. The Cenozoic Southern Ocean: Tectonics, Sedimentation, and Climate Change Between Australia and Antarctica, pp. 5–17.

Cande, S.C., Patriat, P., Dyment, J., 2010. Motion between the Indian, Antarctic and African plates in the early Cenozoic. Geophysical Journal International 183 (1), 127–149.

Chandler, M., Wessel, P., Taylor, B., Seton, M., Kim, S., Hyeong, K., 2012. Reconstructing Ontong Java Nui: implications for Pacific absolute plate motion, hotspot drift and true polar wonder. Earth and Planetary Science Letters 331–332, 140–151.

Charrier, R., Bustamante, M., Comte, D., Elgueta, S., Flynn, J.J., Iturra, N., Muñoz, N., Pardo, M., Thiele, R., Wyss, A.R., 2005. The Abanico extensional basin: regional extension chronology of tectonic inversion and relation to shallow seismic activity and Andean uplift. Neues Jahrbuch für Geologie und Paläontologie 236, 43–77.

Chemenda, A., Lallemand, S., Bokun, A., 2000. Strain partitioning and interplate friction in oblique subduction zones: constraints provided by physical modeling. Journal of Geophysical Research 105, 5567–5582.

Clague, D.A., Dalrymple, G.B., 1987. The Hawaiian-Emperor volcanic chain. Part I. Geologic evolution. Volcanism in Hawaii 1, 5–54.

Cloos, M., 1993. Lithospheric buoyancy and collisional orogenesis: subduction of oceanic plateaus, continental margins, island arcs, spreading ridges and seamounts. Geological Society of America Bulletin 105, 715–737.

Contreras-Reyes, E., Carrizo, D., 2011. Control of high oceanic features and subduction channel on earthquake ruptures along the Chile–Peru subduction zone. Physics of the Earth and Planetary Interiors 186, 49–58.

Cooke, D., Hollings, P., Walshe, J.L., 2005. Giant porphyry deposits – characteristics, distribution and tectonic controls. Economic Geology 100, 801–818.

Cooper, O., Lara, L., 2015. Evolución magmática del complejo volcánico San Félix-San Ambrosio, Pacífico suroriental. XIV Congreso Geológico Chileno, La Serena, octubre 2015.

Courtillot, V., Davaille, A., Besse, J., Stock, J., 2003. Three distinct types of hotspots in the Earth's mantle. Earth and Planetary Science Letters 205, 295–308.

Cox, A., Hart, R., 1986. Plate Tectonics: How It Works. Blackwell, Oxford (Chapters 4 and 7).

Croon, M.B., Cande, S.C., Stock, J.M., 2008. Revised Pacific-Antarctic plate motions and geophysics of the Menard Fracture Zone. Geochemistry, Geophysics, Geosystems 9 (7).

Devey, C., Hekinian, R., Ackermand, D., Binard, N., Francke, B., Hemond, C., Kapsimalis, V., Lorenc, S., Maia, M., Möller, H., Perot, K., Pracht, J., Rogers, T., Stattegger, K., Steinke, S., Victor, P., 1997. The Foundation Seamount Chain: a first survey and sampling. Marine Geology 137, 191–200.

Domínguez, S., Malavieille, J., Lallemand, S.E., 2000. Deformation of accretionary wedges in response to seamount subduction: insights from sandbox experiments. Tectonics 19 (1), 182–196. https://doi.org/10.1029/1999TC900055.

Doubrovine, P.V., Steinberger, B., Torsvik, T.H., 2012. Absolute plate motions in a reference frame defined by moving hot spots in the Pacific, Atlantic, and Indian oceans. Journal of Geophysical Research 117, B09101. https://doi.org/10.1029/2011JB009072.

Espurt, N., Funiciello, F., Martinod, J., Guillaume, B., Regard, V., Faccenna, C., Brusset, S., 2008. Flat subduction dynamics and deformation of the South American plate: insights from analog modeling. Tectonics 27, TC3011. https://doi.org/10.1029/2007TC002175.

Faccenna, C., Oncken, O., Holt, A.F., Becker, T.W., 2017. Initiation of the Andean orogeny by lower mantle subduction. Earth and Planetary Science Letters 463, 189–201.

Farías, M., Charrier, R., Carretier, S., Martinod, J., Fock, A., Campbell, D., Caceres, J., Comte, D., 2008. Late Miocene high and rapid surface uplift and its erosional response in the Andes of central Chile (33–35 S). Tectonics 27 (1).

Gee, J.S., Kent, D.V., 2007. Source of oceanic magnetic anomalies and the geomagnetic polarity time scale. In: Kono, M. (Ed.)Treatise on Geophysics vol. 5. Elsevier, Amsterdam, pp. 455–507 (chap. 12).

Gerya, T., Fossati, D., Cantieni, C., Seward, C., 2009. Dynamic effects of aseismic ridge subduction: numerical modelling. European Journal of Mineralogy 21, 649–661. https://doi.org/10.1127/0935-1221/2009/0021-1931.

González-Ferrán, O., 1987. Evolución geológica de las islas chilenas en el océano Pacífico. Islas oceánicas chilenas: Conocimiento científico y necesidades de investigaciones. Graham, pp. 37–54.

Granot, R., Cande, S.C., Stock, J.M., Damaske, D., 2013. Revised Eocene-Oligocene kinematics for the West Antarctic rift system. Geophysical Research Letters 40 (2), 279–284.

Gutscher, M., Olivet, J., Aslanian, D., Maury, R., Eissen, J., 1999. The 'lost Inca Plateau': cause of the flat subduction beneath Peru? Earth and Planetary Science Letters 168, 255–270.

Gutscher, M., Spakman, W., Bijwaard, H., Engdahl, E., 2000. Geodynamics of flat subduction: seismicity and tomographic constraints from the Andean margin. Tectonics 19 (5), 814–833.

Haase, K.M., Mertz, D.F., Sharp, W.S., Garbe-Schönberg, C.-D., 2000. Sr-Nd-Pb isotope ratios, geochemical compositions, 40Ar/39Ar data of lavas from San Felix island (southeast Pacific): implications for magma genesis and sources. Terra Nova 12, 90–96. https://doi.org/10.1111/j.1365-3121.2000.00278.x.

Hagen, R.A., Moberly, R., 1994. Tectonic effects of a subducting aseismic ridge: the subduction of the Nazca Ridge at the Peru Trench. Marine Geophysical Research 16 (2), 145–161.

Hampel, A., 2002. The migration history of the Nazca Ridge along the Peruvian active margin: a re-evaluation. Earth and Planetary Science Letters 203, 665–679.

Hampel, A., Adam, J., Kukowski, N., 2004. Response of the tectonically erosive south Peruvian forearc to subduction of the Nazca Ridge: analysis of three-dimensional analogue experiments. Tectonics 23 (5), TC5003. https://doi.org/10.1029/2003TC001585.

Hassani, R., Jongmans, D., Chery, J., 1997. Study of plate deformation and stress in subduction processes using two-dimensional numerical models. Journal of Geophysical Research. Solid Earth 102, 17951–17965.

Heine, C., Zoethout, J., Müller, R.D., 2013. Kinematics of the South Atlantic rift. Solid Earth 4, 215–253.

Hey, R., 1977. Tectonic evolution of the Cocos-Nazca spreading center. Geological Society of America Bulletin 88 (10), 1404–1420.

Hochmuth, K., Gohl, K., 2017. Collision of Manihiki Plateau fragments to accretional margins of northern Andes and Antarctic Peninsula. Tectonics 36 (2), 229–240. https://doi.org/10.1002/2016TC004333.
Hoke, L., Lamb, S., 2007. Cenozoic behind-arc volcanism in the Bolivian Andes, South America: implications for mantle melt generation and lithospheric structure. Journal of the Geological Society 164 (4), 795–814.
Hu, J., Liu, L., Hermosillo, A., Zhou, Q., 2016. Simulation of late Cenozoic South American flat-slab subduction using geodynamic models with data assimilation. Earth and Planetary Science Letters 438, 1–13.
Huangfu, P., Wang, Y., Cawood, P.A., Li, Z.H., Fan, W., Gerya, T.V., 2016. Thermo-mechanical controls of flat subduction: insights from numerical modeling. Gondwana Research 40, 170–183.
Husen, S., Kissling, E., Quintero, R., 2002. Tomographic evidence for a subducted seamount beneath the Gulf of Nicoya, Costa Rica: the cause of the 1990 Mw = 7.0 Gulf of Nicoya earthquake. Geophysical Research Letters 29 (8). https://doi.org/10.1029/2001GL014045.
Ito, G., Lin, J., 1995. Oceanic spreading center-hotspot interactions: constraints from along-isochron bathymetric and gravity anomalies. Geology 23, 657–660.
Ito, G., McNutt, M., 1993. Volcanic structure of the Tuamotu island plateau from multi-channel and refraction seismics: evidence for a near ridge origin. International Workshop on the Polynesian Plume Province, Papeete, Tahiti, 1993.
James, D.E., Sacks, S., 1999. Cenozoic formation of the central Andes: a geophysical perspective. In: Skinner, B., et al. (Eds.), Geology and Ore Deposits of the Central Andes. Society of Economic Geologists Special Publication vol. 7. Soc of Econ. Geol., Littleton, Colo, pp. 1–25.
Jordan, T., Isacks, B., Allmendinger, R., Brewer, J., Ramos, V., Ando, C., 1983. Andean tectonics related to geometry of subducted Nazca plate. Geological Society of America Bulletin 94, 341–361.
Jordan, T.E., Burns, W.M., Veiga, R., Pángaro, F., Copeland, P., Kelley, S., Mpodozis, C., 2001. Extension and basin formation in the southern Andes caused by increased convergence rate: a mid-Cenozoic trigger for the Andes. Tectonics 20 (3), 308–324.
Kay, S.M., Abbruzzi, J.M., 1996. Magmatic evidence for Neogene lithospheric evolution of the central Andean "flat-slab" between 30 S and 32 S. Tectonophysics 259, 15–28. https://doi.org/10.1016/0040-1951(96)00032-7.
Kay, S.M., Coira, B., 2009. Shallowing and steepening subduction zones, continental lithospheric loss, magmatism, and crustal flow under the Central Andean Altiplano-Puna Plateau. In: Kay, S.M., Ramos, V.A., Dickenson, W.D. (Eds.), Backbone of the Americas: Shallow Subduction, Plateau Uplift, and Ridge and Terrane Collision: Geological Society of America Memoirs. 204, pp. 229–259. https://doi.org/10.1130/2009.1204 (11).
Kay, S.M., Mpodozis, C., Coira, B., 1999. Magmatism, tectonism, and mineral deposits of the Central Andes (22°–33°S latitude). In: Skinner, B.J. (Ed.), Geology and Ore Deposits of the Central Andes. Society of Economic Geology Special Publication vol. 7, pp. 27–59.
Kay, S.M., Coira, B., Mpodozis, C., 2008. Field Trip Guide: Neogene Evolution of the Central Andean Puna Plateau and Southern Central Volcanic Zone. Geological Society of America, pp. 119–183.
Kerr, A.C., Tarney, J., 2005. Tectonic evolution of the Caribbean and northwestern South America: the case for accretion of two Late Cretaceous oceanic plateaus. Geology 33 (4), 269–272.
Kerr, A.C., Aspden, J., Tarney, J., Pilatasig, L., 2002. The nature and provenance of accreted oceanic terranes in western Ecuador: geochemical and tectonic constraints. Journal of the Geological Society 159, 577–594. https://doi.org/10.1144/0016-764901-151.
Kingsley, R.H., Schilling, J.G., 1998. Plume-ridge interaction in the Easter-Salas y Gomez seamount chain-Easter Microplate system: Pb isotope evidence. Journal of Geophysical Research, Solid Earth 103 (B10), 24159–24177.
Kodaira, S., Takahashi, N., Nakanishi, A., Miura, S., Kaneda, Y., 2000. Subducted seamount imaged in the rupture zone of the 1946 Nankaido earthquake. Science 289 (5476), 104–106. https://doi.org/10.1126/science.289.5476.104.
Kopp, H., Flueh, E.R., Papenberg, C., Klaeschen, D., 2004. Seismic investigations of the O'Higgins Seamount Group and Juan Fernández ridge: aseismic ridge emplacement and lithosphere hydration. Tectonics 23 (2), 1–21. https://doi.org/10.1029/2003TC001590.
Koppers, A.A., Watts, A.B., 2010. Intraplate seamounts as a window into deep Earth processes. Oceanography 23 (1), 42–57.
Lamb, S., Hoke, L., 1997. Origin of the high plateau in the central Andes, South America. Tectonics 16, 623–649.
Lamb, S., Hoke, L., Kennan, L., Dewey, J., 1997. Cenozoic evolution of the central Andes in Bolivia and northern Chile. Geological Society of London, Special Publication 121, 237–264. https://doi.org/10.1144/GSL.SP.1997.121.01.10.
Larson, R.L., 1991. Latest pulse of Earth: evidence for a mid-Cretaceous superplume. Geology 19 (6), 547–550.
Larson, R.L., Pockalny, R., 1997. Changing triple junctions in the mid-Cretaceous: from the Nova Canton Trough to Tongareva Atoll. Eos, Transactions of the American Geophysical Union (Fall Supplement), F721.
Larson, R.L., Pockalny, R., Viso, R., Erba, E., Abrams, L., Luyendyk, B., Stock, J., Clayton, R., 2002. Mid-Cretaceous tectonic evolution of the Tongareva triple junction in the Southwestern Pacific basin. Geology 30, 67–70.
Liu, Z., 1996. The Origin and Evolution of the Easter Seamount Chain. University of South Florida, St. Petersburg (PhD thesis, 266 pp.).
Lonsdale, P., 2005. Creation of the Cocos and Nazca plates by fission of the Farallon plate. Tectonophysics 404 (3), 237–264.
Luzieux, L.D.A., 2007. Origin and Late Cretaceous-Tertiary Evolution of the Ecuadorian Forearc. Institute of Geology ETH Zürich, Switzerland (PhD Thesis).
Mammerickx, J., 1992. The Foundation seamounts: tectonic setting of a newly discovered seamount chain in the South Pacific. Earth and Planetary Science Letters 113, 293–306.
Manea, V.C., Gurnis, M., 2007. Subduction zone evolution and low viscosity wedges and channels. Earth and Planetary Science Letters 264 (1–2), 22–45.
Manea, V.C., Pérez-Gussinyé, M., Manea, M., 2012. Chilean flat slab subduction controlled by overriding plate thickness and trench rollback. Geology 40 (1), 35–38.
Marks, K.M., Tikku, A.A., 2001. Cretaceous reconstructions of East Antarctica, Africa and Madagascar. Earth and Planetary Science Letters 186 (3–4), 479–495.
Martinod, J., Funiciello, F., Faccenna, C., Labanieh, S., Regard, V., 2005. Dynamical effects of subducting ridges: insights from 3-D laboratory models. Geophysical Journal International 163, 1137–1150.
Martinod, J., Husson, L., Roperch, P., Guillaume, B., Espurt, N., 2010. Horizontal subduction zones, convergence velocity and the building of the Andes. Earth and Planetary Science Letters 299, 299–309. https://doi.org/10.1016/j.epsl.2010.09.010.
Matthews, K.J., Müller, R.D., Wessel, P., Whittaker, J.M., 2011. The tectonic fabric of the ocean basins. Journal of Geophysical Research, Solid Earth 116 (B12).
Matthews, K.J., Williams, S.E., Whittaker, J.M., Müller, R.D., Seton, M., Clarke, G.L., 2015. Geologic and kinematic constraints on Late Cretaceous to mid Eocene plate boundaries in the southwest Pacific. Earth-Science Reviews 140, 72–107.
Mayes, C.L., Lawver, L.A., Sandwell, D.T., 1990. Tectonic history and new isochron chart of the South Pacific. Journal of Geophysical Research 95, 8543–8567.
McGeary, S., Nur, A., Ben-Avraham, Z., 1985. Spatial gaps in arc volcanism: the effect of collision or subduction of oceanic plateaus. Tectonophysics 119, 195–221.
McNutt, M., Bonneville, A., 2000. A shallow, chemical origin for the Marquesas Swell. Geochemistry, Geophysics, Geosystems 1 (6). https://doi.org/10.1029/1999GC00002.
McNutt, M., Caress, D., Reynolds, J., Jordahl, K., Duncank, R., 1997. Failure of plume theory to explain midplate volcanism in the southern Austral islands. Nature 389, 479–482.
McQuarrie, N., 2002. The kinematic history of the central Andean fold-thrust belt, Bolivia: implications for building a high plateau. Geological Society of America Bulletin 114 (p), 950–963. https://doi.org/10.1130/0016-7606(2002)114<0950:TKHOTC>2.0.CO;2.
Montelli, R., Nolet, G., Dahlen, F.A., Masters, G., 2006. A catalogue of deep mantle plumes: new results from finite-frequency tomography. Geochemistry, Geophysics, Geosystems 7, Q11007. https://doi.org/10.1029/2006GC001248.
Morgan, W.J., 1972. Deep mantle convection plumes and plate motions. The American Association of Petroleum Geologists Bulletin 56, 203–213.
Morgan, W.J., 1978. Rodriguez, Darwin, Amsterdam, …, a second type of hotspot island. Journal of Geophysical Research. Solid Earth 83 (B11), 5355–5360. https://doi.org/10.1029/2003JB002431.
Müller, R.D., Roest, W., Royer, J., 1998. Asymmetric sea-floor spreading caused by ridge-plume interactions. Nature 396, 455–459.
Müller, R.D., Royer, J.Y., Cande, S.C., Roest, W.R., Maschenkov, S., 1999. New constraints on the Late Cretaceous/Tertiary plate tectonic evolution of the Caribbean. Sedimentary Basins of the World vol. 4. Elsevier, pp. 33–59.
Müller, R.D., Sdrolias, M., Gaina, C., Roest, W.R., 2008. Age, spreading rates, and spreading asymmetry of the world's ocean crust. Geochemistry, Geophysics, Geosystems 9 (4).
Müller, R.D., Seton, M., Zahirovic, S., Williams, S., Matthews, K., Wright, N., Shephard, G., Maloney, K., Barnett-Moore, N., Hosseinpour, M., Bower, D., Cannon, J., 2016. Ocean basin evolution and global-scale plate reorganization events since Pangea breakup. Annual Review of Earth and Planetary Sciences 44, 107–138.
Muñoz-Sáez, C., Pinto, L., Charrier, R., Nalpas, T., 2014. Influence of depositional load on the development of a shortcut fault system during the inversion of an extensional basin: the Eocene Oligocene Abanico Basin case, central Chile Andes (33°–35°S). Andean Geology 41 (1), 1–28 (2014).
Naar, D.F., Hey, R.N., 1986. Fast rift propagation along the East Pacific Rise near Easter Island. Journal of Geophysical Research, Solid Earth 91 (B3), 3425–3438.
Naar, D.F., Hey, R.N., 1991. Tectonic evolution of the Easter microplate. Journal of Geophysical Research 96, 7961–7993.
Nankivell, A.P., 1997. Tectonic Evolution of the Southern Ocean Between Antarctica, South America and Africa Over the Past 84 Ma. University of Oxford (Doctoral dissertation).
O'Connor, J., Stoffers, P., Wijbrans, J., 1998. Migration rate of volcanism along the Foundation Chain, SE Pacific. Earth and Planetary Science Letters 164, 41–59.
Okal, E.A., Cazenave, A., 1985. A model for the plate tectonic evolution of the east-central Pacific based on SEASAT investigations. Earth and Planetary Science Letters 72 (1), 99–116.
Oncken, O., Hindle, D., Kley, J., Elger, P., Victor, P., Schemmann, K., 2006. Deformation of the Central Andean upper plate system—facts, fiction, and constraints for plateau models. In: Oncken, O., et al. (Eds.), The Andes. Springer, pp. 3–28.
Orellana-Rovirosa, F., Richards, M., 2017. Rough versus smooth topography along oceanic hotspot tracks: observations and scaling analysis. Geophysical Research Letters 44 (9), 4074–4081. https://doi.org/10.1002/2016GL072008.
Pilger, R.H., 1981. Plate reconstructions, aseismic ridges, and low-angle subduction beneath the Andes. Geological Society of America Bulletin 92, 448–456.
Pilger, R.H., 1984. Cenozoic plate kinematics, subduction and magmatism: South American Andes. Journal of the Geological Society 141, 793–802. https://doi.org/10.1144/gsjgs.141.5.0793.
Pinet, N., Cobbold, P.R., 1992. Experimental insights into the partitioning of motion within zones of oblique subduction. Tectonophysics 206, 371–388.
Pubellier, M., Cobbold, P.R., 1996. Analogue models for the transpressional docking of volcanic arcs in the western Pacific. Tectonophysics 253 (1–2), 33–52.
Ramos, V., Folguera, A., 2009. Andean flat-slab subduction through time. Geological Society of London, Special Publication 327, 31–54. https://doi.org/10.1144/SP327.3.
Ray, S.J., Mahoney, J., Duncan, R., Ray, J., Wessel, P., Naarm, D., 2012. Chronology and geochemistry of lavas from the Nazca Ridge and Easter Seamount Chain: a 30 Myr hotspot record. Journal of Petrology, 1–32 https://doi.org/10.1093/petrology/egs021.
Reyes, J., Lara, L.E., 2012. Juan Fernández Ridge (Nazca Plate): petrology and thermochronology of a rejuvenated hotspot trail. EGU General Assembly Conference Abstracts vol. 14, p. 6145 (2012, April).

Richards, M.A., Contreras-Reyes, E., Lithgow-Bertelloni, C., Ghiorso, M., Stixrude, L., 2013. Petrological interpretation of deep crustal intrusive bodies beneath oceanic hotspot provinces. Geochemistry, Geophysics, Geosystems 14, 604–619. https://doi.org/10.1029/2012GC004448.

Robinson, D.P., Das, S., Watts, A.B., 2006. Earthquake rupture stalled by a subducting fracture zone. Science 312 (5777), 1203–1205. https://doi.org/10.1126/science.1125771.

Rodríguez-González, J., Negredo, A.M., Billen, M.I., 2012. The role of the overriding plate thermal state on slab dip variability and on the occurrence of flat subduction. Geochemistry, Geophysics, Geosystems 13 (1).

Roperch, P., Sempere, T., Macedo, O., Arriagada, C., Fornari, M., Tapia, C., Garcia, M., Laj, C., 2006. Counterclockwise rotation of late Eocene–Oligocene fore-arc deposits in southern Peru and its significance for oroclinal bending in the central Andes. Tectonics 25 (3).

Roperch, P., Carlotto, V., Ruffet, G., Fornari, M., 2011. Tectonic rotations and transcurrent deformation south of the Abancay deflection in the Andes of southern Peru. Tectonics 30 (2).

Rosenbaum, G., Mo, W., 2011. Tectonic and magmatic responses to the subduction of high bathymetric relief. Gondwana Research 19 (3), 571–582.

Rosenbaum, G., Giles, D., Saxon, M., Betts, P.G., Weinberg, R., Duboz, C., 2005. Subduction of the Nazca Ridge and the Inca Plateau: insights into the formation of ore deposits in Peru. Earth and Planetary Science Letters 239, 18–32.

Rowan, C., Rowley, D., 2014. Spreading behaviour of the Pacific-Farallon ridge system since 83 Ma. Geophysical Journal International 197, 1273–1283. https://doi.org/10.1093/gji/ggu056.

Royer, J.Y., Chang, T., 1991. Evidence for relative motions between the Indian and Australian plates during the last 20 my from plate tectonic reconstructions: implications for the deformation of the Indo-Australian plate. Journal of Geophysical Research, Solid Earth 96 (B7), 11779–11802.

Sallarès, V., Charvis, P., Flueh, E.R., Bialas, J., 2003. Seismic structure of Cocos and Malpelo Volcanic Ridges and implications for hotspot-ridge interaction. Journal of Geophysical Research, Solid Earth 108 (B12).

Schellart, W.P., 2017. Andean mountain building and magmatic arc migration driven by subduction-induced whole mantle flow. Nature Communications 8 (1), 2010.

Schellart, W.P., Rawlinson, N., 2013. Global correlations between maximum magnitudes of subduction zone interface thrust earthquakes and physical parameters of subduction zones. Physics of the Earth and Planetary Interiors 225, 41–67. https://doi.org/10.1016/j.pepi.2013.10.001.

Schepers, G., Van Hinsbergen, D.J., Spakman, W., Kosters, M.E., Boschman, L.M., McQuarrie, N., 2017. South-American plate advance and forced Andean trench retreat as drivers for transient flat subduction episodes. Nature Communications 8, 15249.

Scheuber, E., Reutter, K.-J., 1992. Magmatic arc tectonics in the Central Andes between 21° and 25°S. In: Oliver, R.A., Vatin-Perignon, N., Laubacher, G. (Eds.), Andean Geodynamics. Tectonophysics vol. 205, pp. 127–140.

Scholz, C.H., Small, C., 1997. The effect of seamount subduction on seismic coupling. Geology 25 (6), 487–490. https://doi.org/10.1130/0091-7613(1997)025<0487:TEOSSO>2.3.CO;2.

Seton, M., Müller, R.D., Zahirovic, S., Gaina, C., Torsvik, T., Shephard, G., Talsma, A., Gurnis, M., Turner, M., Maus, S., Chandler, M., 2012. Global continental and ocean basin reconstructions since 200 Ma. Earth-Science Reviews 113 (3–4), 212–270.

Seton, M., Whittaker, J., Wessel, P., Müller, R., DeMets, C., et al., 2014. Community infrastructure and repository for marine magnetic identifications. Geochemistry, Geophysics, Geosystems 15, 1629–1641.

Silver, P., Russo, R., Lithgow-Bertelloni, C., 1998. Coupling of South American and African plate motion and plate deformation. Science 279, 60–63.

Skinner, S.M., Clayton, R.W., 2013. The lack of correlation between flat slabs and bathymetric impactors in South America. Earth and Planetary Science Letters 371, 1–5.

Small, C., 1995. Observations of ridge–hotspot interactions in the Southern Ocean. Journal of Geophysical Research 100, 17931–17946.

Smalley, R., Pujol, J., Regnier, M., Chiu, J., Chatelain, J., Isacks, B., Araujo, M., Puebla, N., 1993. Basement seismicity beneath the Andean Precordillera thin skinned thrust belt and implications for crustal and lithospheric behavior. Tectonics 12, 63–76.

Somoza, R., 1998. Updated Nazca (Farallon)-South America relative motions during the last 40 My: implications for mountain building in the central Andean region. Journal of South American Earth Sciences 11 (3), 211–215.

Spikings, R.A., Simpson, G., 2014. Rock uplift and exhumation of continental margins by the collision, accretion, and subduction of buoyant and topographically prominent oceanic crust. Tectonics 33. https://doi.org/10.1002/2013TC003425.

Spikings, R.A., Seward, D., Winkler, W., Ruiz, G.M., 2000. Low temperature thermochronology of the northern Cordillera Real, Ecuador tectonic insights from zircon and apatite fission-track analysis. Tectonics 19, 649–668.

Spikings, R.A., Winkler, W., Seward, D., Handler, R., 2001. Along-strike variations in the thermal and tectonic response of the continental Ecuadorian Andes to the collision with heterogeneous oceanic crust. Earth and Planetary Science Letters 186, 57–73.

Spikings, R.A., Winkler, W., Hughes, R.A., Handler, R., 2005. Thermochronology of allochthonous blocks in Ecuador: unraveling the accretionary and post-accretionary history of the Northern Andes. Tectonophysics 399, 195–220.

Steinberger, B., 2000. Plumes in a convecting mantle: models and observations for individual hotspots. Journal of Geophysical Research, Solid Earth 105 (B5), 11127–11152.

Steinberger, B., 2002. Motion of the Easter hotspot relative to Hawaii and Louisville hotspots. Geochemistry, Geophysics, Geosystems 3 (11), 8503. https://doi.org/10.1029/2002GC000334.

Steinberger, B., Antretter, M., 2006. Conduit diameter and buoyant rising speed of mantle plumes: implications for the motion of hot spots and shape of plume conduits. Geochemistry, Geophysics, Geosystems 7 (11).

Steinberger, B., O'Connell, R.J., 1998. Advection of plumes in mantle flow: implications for hotspot motion, mantle viscosity and plume distribution. Geophysical Journal International 132 (2), 412–434.

Sun, M., Ling, M., Yang, X., Fan, W., Ding, X., Liang, H., 2010. Ridge subduction and porphyry copper-gold mineralization: an overview. Science China Earth Sciences 53 (4), 475–484. https://doi.org/10.1007/s11430-101-0024-0.

Taylor, B., 2006. The single largest oceanic plateau: Ontong Java-Manihiki-Hikurangi. Earth and Planetary Science Letters 241, 372–380.

Tebbens, S., Cande, S., 1997. Southeast Pacific tectonic evolution from early Oligocene to present. Journal of Geophysical Research 102 (B6), 12061–12084.

Vallejo, C., 2007. Evolution of the Western Cordillera in the Andes of Ecuador (Late Cretaceous-Paleogene). Institute of Geology ETH Zürich, Switzerland (PhD Thesis).

van Hunen, J., van den Berg, A.P., Vlaar, N.J., 2000. A thermo-mechanical model of horizontal subduction below an overriding plate. Earth and Planetary Science Letters 182, 157–169.

van Hunen, J., van den Berg, A.P., Vlaar, N.J., 2002. On the role of subducting oceanic plateaus in the development of shallow flat subduction. Tectonophysics 352, 317–333.

Viso, R.F., Larson, R.L., Pockalny, R.A.-., 2005. Tectonic evolution of the Pacific-Phoenix-Farallon triple junction in the South Pacific Ocean. Earth and Planetary Science Letters 233, 179–194.

Vogt, K., Gerya, T., 2014. From oceanic plateaus to allochthonous terranes: numerical modelling. Gondwana Research 25 (2014), 494–508.

von Huene, R., Corvalán, J., Flueh, E., Hinz, K., Korstgard, J., Ranero, C., Weinrebe, W., the CONDOR Scientists, 1997. Tectonic control of the subducting Juan Fernández Ridge on the Andean margin near Valparaiso, Chile. Tectonics 16 (3), 474–488.

Wessel, P., Kroenke, L., 2000. Ontong Java plateau and late Neogene changes in Pacific plate motion. Journal of Geophysical Research 105 (B12), 28255–28278. https://doi.org/10.1029/2000JB900290.

Wessel, P., Kroenke, L., 2008. Pacific absolute plate motion since 145 Ma: an assessment of the fixed hotspot hypothesis. Journal of Geophysical Research 113, B06101.

Woods, M.T., Okal, E.A., 1994. The structure of the Nazca ridge and Sala y Gomez seamount chain from the dispersion of Rayleigh waves. Geophysical Journal International 117, 205–222.

Wright, N.M., Müller, R.D., Seton, M., Williams, S.E., 2015. Revision of Paleogene plate motions in the Pacific and implications for the Hawaiian-Emperor bend. Geology 43 (5), 455–458.

Wright, N.M., Seton, M., Williams, E., Müller, R.D., 2016. The late Cretaceous to recent tectonic history of the Pacific Ocean basin. Earth Science Reviews 154. https://doi.org/10.1016/j.earscirev.2015.11.015 (2015).

Yáñez, G., Ranero, C., von Huene, R., Díaz, J., 2001. Magnetic anomaly interpretation across the southern central Andes (32°–34°S): the role of the Juan Fernández Ridge in the late Tertiary evolution of the margin. Journal of Geophysical Research 106 (B4), 6325–6345.

Yáñez, G., Cembrano, J., Pardo, M., Ranero, C., Selles, D., 2002. The Challenger-Juan Fernández-Maipo major tectonic transition of the Nazca-Andean subduction system at 33–34°S: geodynamic evidence and implications. Journal of South American Earth Sciences 15, 23–38.